

Automating the determination of tight-binding representations for two-dimensional ferroelectrics

An Honors Thesis submitted in partial
fulfillment of the requirements for
Honors Studies in Physics

By

Joseph E. Roll

Spring 2023
Physics
Fulbright College of Arts and Sciences
The University of Arkansas

Acknowledgements

Above all, I want to thank Dr. Salvador Barraza-Lopez for his support over the past three years. I joined his group in the Summer of 2020 and he has provided constant guidance since, opening many doors with respect to coursework and research opportunities. He has helped me become nationally competitive with our work, and I will continue my academic career at the University of Texas at Austin, a top university. For all of this, I am forever grateful.

I also thank Dr. Jack Villanova and Dr. Shiva Poudel for their help in this project and many others over the years. I also thank Dr. Debajit Chakraborty and Luis Enrique Rosas Hernandez for their current contributions to this project.

Finally, I want to thank my amazing parents and friends. They have provided invaluable support for my dream of being a Physicist, which has never been easy. Without them, I doubt I would be able to realize this dream; thank you all.

Contents

1 Motivation	4
2 Condensed matter physics	5
2.1 What is a crystal?	5
2.2 Common coordinate systems	6
3 Density functional theory	8
3.1 Brief explanation	8
3.2 Choice of basis	9
3.3 Advanced techniques	10
3.3.1 Green's functions	10
3.3.2 Screened Coulomb interactions	11
3.3.3 GW approximations	12
4 Structural determination and analysis	13
4.1 Atomistic structure	13
4.2 Symmetry analysis	14
4.3 Matrix representation	14
4.4 Algorithm to check for inversion symmetry	15
5 Calculating the electronic structure	18
5.1 Plane wave basis	18
5.1.1 Without GW approximations	18
5.1.2 With GW approximations	20
5.2 Numerical atomic orbital basis	23
6 Creating a tight-binding representation	29
6.1 Linear combination of atomic orbitals	29
6.1.1 SnS: single zeta basis	32
6.1.2 SnS: single zeta polarized basis	36
6.1.3 SnTe: single zeta basis	43
6.1.4 SnTe: single zeta polarized basis	47
7 Determining tight-binding parameters	54
7.1 Required data files	54
7.2 Systems of equations	55

8 Future developments	58
A Algorithm to check inversion symmetry	59
B Slater-Koster expressions for tight-binding representations	65

Chapter 1

Motivation

After the discovery of graphene and its extraordinary properties in 2004 [1], which later earned a Nobel Prize in Physics in 2010, the study of atomically thin materials, also known as monolayers, has grown tremendously. That focus includes both theoretical and experimental investigations to determine the stability and properties of different monolayers. While many of these monolayers are only comprised of one element—such as graphene [1], black phosphorus [2, 3], and silicene [4, 5]—some are comprised of two elements.

These two-element (binary) materials include hexagonal boron nitride monolayers [6, 7] and transition-metal dichalcogenide monolayers [8, 9]. These two material families are particularly interesting because of their crystal symmetries, or lack thereof. These materials do not have an inversion center, which is a point in space where atoms of a given element can be related to one another by an inversion through that point. Not having this symmetry leads to a spontaneous electric polarization of the material, similar to polar molecules such as water. Interestingly, in some other binary materials the direction of this electric dipole can be reversed by applying an external electric field [10, 11]. That has become increasingly important for compact memory storage within electrical devices and for energy harvesting. For the sake of classifications, materials with this property are called *ferroelectric*.

A promising family of ferroelectric materials is group-IV monochalcogenide monolayers (MX), which are comprised of one 4A metal and one 6A chalcogen (i.e., GeS and SnSe) [12]. For these materials, its lack of inversion center leads to interesting light-matter interactions such as large second-harmonic generation (SHG). SHG is where two incident photons with some frequency (ω) enter a material, but only one leaves with double the original frequency (2ω). That property is particularly useful within optics and laser physics, as it lets researchers better control light.

While studies on GeS and SnSe exist [13, 14], it is still unknown how the intrinsic polarization of these materials affects their SHG. We can explore that through the use of tight-binding representations which allow for accurate and cheap computational modeling of material properties. We develop a process here to determine tight-binding representations and apply it to several group-IV monochalcogenide monolayers.

Chapter 2

Condensed matter physics

2.1 What is a crystal?

As shown in introductory chemistry courses, all materials are made of atoms. Where these atoms are located in a material can greatly change its properties. In studying how atoms position themselves in materials, there are two classifications:

- *Amorphous materials*: atoms are positioned randomly (without a repeating pattern). This is seen in glass or gel.
- *Crystal materials*: atoms have a repeating pattern, called a crystal structure. This is seen in table salt (NaCl).

This study focuses on crystal materials, a.k.a. crystals, where their atoms have a repeating pattern. The pattern that actually repeats is called the unit cell and is exemplified in Figure 2.1. A unit cell is defined by vectors called *lattice vectors*, denoted $\{\mathbf{a}_1, \mathbf{a}_2, \mathbf{a}_3\}$ which span our material. These are special because if there is an atom at some position τ , there will be another atom of the same element at $\tau + m_1\mathbf{a}_1 + m_2\mathbf{a}_2 + m_3\mathbf{a}_3$ for $m_i \in \mathbb{Z}$.

It is important to know that crystals are not always one huge block of interconnected atoms (like with table salt). Sometimes crystals are made of many distinct layers of atoms, like onions and Shrek [15], whose layers are held together by van der Waals forces. In this case, as interlayer attractions are weaker than intralayer attractions, one can simply rip these layers apart until only one remains. This process is actually common in laboratory settings using Scotch tape, but with the more sophisticated name of *exfoliation*. This one resultant layer, a monolayer, creates the foundation of our studies.

Even if one knows the chemical make-up of a material, the atomistic structure is still important. This is easily seen when comparing graphite (pencil lead) and diamond. Both materials are composed of solely carbon atoms, but have wildly different properties. This is due to their different structures; graphite is many layers of carbon while diamond is a huge block of interconnected atoms. This idea is also seen with temperature dependent studies, where material properties change depending on the temperature [16]. As the chemical formula for

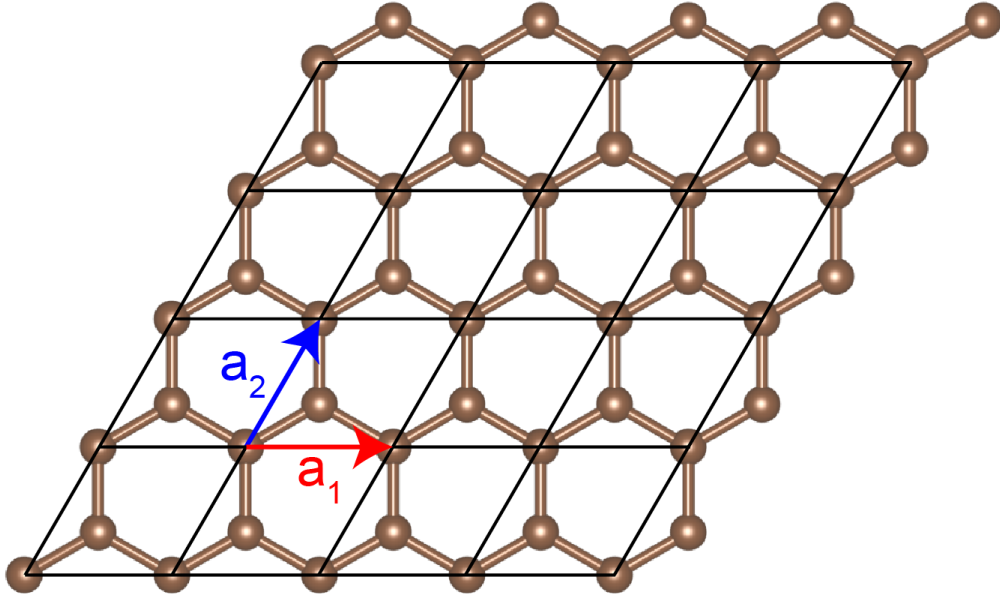


Figure 2.1: Graphene atomistic structure. This shows the periodic nature of crystals, where lattice vectors (\mathbf{a}_1 and \mathbf{a}_2) are also shown. Note there is no need for \mathbf{a}_3 as this specific material is planar (perfectly two-dimensional). Thus our lattice vectors must only span two dimensions.

the material doesn't change (with respect to temperature), the resultant structural change must be effecting these properties.

2.2 Common coordinate systems

When working with crystals, specifically with atomistic positions, there are two popular coordinate systems. The first, and more intuitive option, is *cartesian coordinates* (denoted by a subscript c). One must first define an origin and where $\hat{\mathbf{x}}$ and $\hat{\mathbf{y}}$ are pointing. Then the positions of all atoms can be expressed as

$$\mathbf{r} = \begin{pmatrix} x \\ y \\ z \end{pmatrix}_c = x \begin{pmatrix} 1 \\ 0 \\ 0 \end{pmatrix} + y \begin{pmatrix} 0 \\ 1 \\ 0 \end{pmatrix} + z \begin{pmatrix} 0 \\ 0 \\ 1 \end{pmatrix} = x\hat{\mathbf{x}} + y\hat{\mathbf{y}} + z\hat{\mathbf{z}} \quad (2.1)$$

for some $(x, y, z) \in \mathbb{R}^3$. But for many cases it is much more convenient to use *direct coordinates* (denoted with a subscript d). Instead of our standard Euclidean basis, we use our lattice vectors as introduced to define crystalline periodicity. So the positions of all atoms can be expressed as

$$\mathbf{r} = \begin{pmatrix} x \\ y \\ z \end{pmatrix}_d = x\mathbf{a}_1 + y\mathbf{a}_2 + z\mathbf{a}_3. \quad (2.2)$$

We know such x , y , and z exist for our direct coordinates because our set of lattice vectors must span the material. To show how this new choice can simplify calculations, an atom is within our unit cell if $\mathbf{r} = (x, y, z)_d^T$ such that $0 \leq x, y, z \leq 1$. To switch between the two bases, we can see

$$\mathbb{A} := \begin{pmatrix} | & | & | \\ \mathbf{a}_1 & \mathbf{a}_2 & \mathbf{a}_3 \\ | & | & | \end{pmatrix} \quad : \quad \mathbb{A}\mathbf{x}_d = \mathbf{x}_c \iff \mathbb{A}^{-1}\mathbf{x}_c = \mathbf{x}_d. \quad (2.3)$$

Chapter 3

Density functional theory

3.1 Brief explanation

When studying molecules and materials, there are often many electrons and ions which interact. Quantum mechanics requires the use of the many-body (time-independent) Schrödinger equation

$$\hat{H}\Psi(\mathbf{r}_1, \mathbf{r}_2, \dots, \mathbf{r}_N) = E\Psi(\mathbf{r}_1, \mathbf{r}_2, \dots, \mathbf{r}_N) \text{ such that}$$

$$\hat{H} := (\hat{T} + \hat{V} + \hat{U}) = \sum_i \left(-\frac{\hbar^2}{2m_i} \nabla_i^2 \right) + \sum_i V(\mathbf{r}_i) + \sum_{i \neq j} \frac{e^2}{|\mathbf{r}_i - \mathbf{r}_j|}. \quad (3.1)$$

Here the first term (\hat{T}) is from the kinetic energy of the electrons, the second term (\hat{V}) is from the potential felt by electrons from the nuclei, and the third term (\hat{U}) is from electron-electron interactions [17]. Problems arise when approaching this computationally; for N electrons, the required storage scales as (# of grid points) N . So for a five electron system on a $10 \times 10 \times 10$ grid, this will require about 10 petabytes of memory [18]. This is very limiting, as many materials have more than five total electrons and this is a coarse grid. A solution to this issue is through the method proposed by Kohn and Sham [19]: to replace this many-body problem with a single electron problem. Instead of one wavefunction of N position vectors, we use N wavefunctions of one position vector which scales as $N \times$ (# of grid points) [18]. This takes the form of a basis set $\{\psi_i(\mathbf{r})\}_{i=1}^N$ such that

$$\Psi(\mathbf{r}_1, \mathbf{r}_2, \dots, \mathbf{r}_N) = \prod_{i=1}^N \psi_i(\mathbf{r}). \quad (3.2)$$

Our choice of basis set is extremely important and will be expanded upon later in this section. To ensure similar results no matter the basis set, we first make sure that the electron density (hence *density* functional theory (DFT)) matches between the many-body and single-electron systems

$$\rho(\mathbf{r}) = N \int d\mathbf{r}_2 \cdots \int d\mathbf{r}_N \Psi^*(\mathbf{r}, \mathbf{r}_2, \dots, \mathbf{r}_N) \Psi(\mathbf{r}, \mathbf{r}_2, \dots, \mathbf{r}_N) = \sum_{i=1}^N |\psi_i(\mathbf{r})|^2. \quad (3.3)$$

This now turns into an optimization problem, where we want to minimize the energy functional (hence density *functional* theory) [19] defined as

$$E[\rho] := \langle \Psi[\rho] | \hat{T} + \hat{V} | \Psi[\rho] \rangle. \quad (3.4)$$

Note this minimization doesn't include explicit electron-electron interactions (\hat{U}) as we have a single-electron model. This normally does not cause many issues but does for our specific case of light-matter interactions. As such, this issue is discussed in Sections 3.3.3 and 5.1.2. In doing this minimization, we can rewrite Eqn (3.1) as

$$\left[-\frac{\hbar^2}{2m_e} \nabla^2 + V(\mathbf{r}) + \int d\mathbf{r}' \frac{\rho(\mathbf{r}')}{|\mathbf{r} - \mathbf{r}'|} + V_{XC}(\mathbf{r}) \right] \psi_i(\mathbf{r}) = \epsilon_i \psi_i(\mathbf{r}) \quad (3.5)$$

for all i . But what is V_{XC} ? This is the exchange-correlation (pseudo)potential and will change depending on our needs. There is an entire field of study into creating these, and there are many different options available to researchers. As the intricate study of pseudopotentials is beyond the scope of this thesis (it falls more onto chemists than physicists), we will simply state which V_{XC} is chosen for each purpose.

3.2 Choice of basis

Another way to dramatically increase computational efficiency is to exploit the symmetries of our system. While there are many possibilities, all crystalline structures have translational symmetry by definition. This leads to a periodic potential within our Schrödinger equation. Bloch's theorem shows that given some Bloch vector \mathbf{k} ,

$$\psi_{n,\mathbf{k}}(\mathbf{r} + \mathbf{R}) = \psi_{n,\mathbf{k}}(\mathbf{r}) e^{i\mathbf{k}\cdot\mathbf{R}} \quad (3.6)$$

for any $\mathbf{R} = m_1 \mathbf{a}_1 + m_2 \mathbf{a}_2 + m_3 \mathbf{a}_3$ such that $m_i \in \mathbb{Z}$. Here n is our *band index* and runs over all electrons within the unit cell. Our Bloch vector is also restricted to the first Brillouin zone (BZ), which once again helps us computationally. Within our unit cell, we then know that

$$\psi_{n,\mathbf{k}}(\mathbf{r}) = u_n(\mathbf{r}) e^{i\mathbf{k}\cdot\mathbf{r}} \text{ where } u_n(\mathbf{r} + \mathbf{R}) = u(\mathbf{r}). \quad (3.7)$$

This exponential term 'folds' our wavefunction back into the unit cell.

As stated before, our choice of basis function is extremely important. One popular choice is *plane waves*. This sets

$$\psi_{n,\mathbf{k}}(\mathbf{r}) = \frac{1}{\Omega^{1/2}} \sum_{\mathbf{G}} C_{\mathbf{G},n,\mathbf{k}} e^{i(\mathbf{k}+\mathbf{G})\cdot\mathbf{r}} \quad u_{n,\mathbf{k}}(\mathbf{r}) = \frac{1}{\Omega^{1/2}} \sum_{\mathbf{G}} C_{\mathbf{G},n,\mathbf{k}} e^{i\mathbf{G}\cdot\mathbf{r}} \quad (3.8)$$

where $\Omega := \mathbf{a}_1 \cdot (\mathbf{a}_2 \times \mathbf{a}_3)$ is the unit cell volume, and \mathbf{G} are linear combinations (in \mathbb{Z}) of reciprocal lattice vectors. So that we don't add up infinitely many \mathbf{G} vectors, they all

must satisfy $\frac{\hbar^2}{2m}|\mathbf{G} + \mathbf{k}|^2 < E_{cutoff}$ for some given cutoff energy [18, 20]. Reciprocal lattice vectors which do not satisfy this can also be used in other cases such as scattering theory; this leads to exponentially decaying (evanescent) waves. This basis set is very accurate but computationally expensive.

Another popular choice is *numerical atomic orbitals*. This sets each basis function to some numerical approximation for one-electron atomic orbitals (s, p, d, f). This method also sets a cutoff radius with which our wavefunction and potential vanish [21, 22]. While this is less accurate than the plane wave basis, it is much cheaper computationally and allows for more freedom when manipulating our Hamiltonian matrix.

3.3 Advanced techniques

This section is effectively a summary of notes presented at a VASP workshop at the National Energy Research Scientific Computing Center (NERSC) by Martijn Marsman. It is a great resource where the notes, and corresponding talk, are free to view online [23]. This specific implementation relies heavily on several works [24, 25, 26, 27, 28].

3.3.1 Green's functions

We will now correct the issues caused by ignoring electron-electron interactions. To do so, we will use perturbation theory with Green's functions. The first question to ask is: what is perturbation theory? For didactic purposes, let H_0 be a sufficiently simple system such that we can find its eigenpairs (eigenvalues and eigenvectors/eigenfunctions for $H_0\psi_{i,0} = \epsilon_i\psi_{i,0}$). Now let $H_0 + \delta$ be a more complicated system such that we can no longer solve it using normal methods. Assuming that the effects of δ are small (hence a small *perturbation*) we can use perturbation theory. It is a multi-step process:

1. Find the eigenvectors/eigenfunctions for our simpler system, H_0 . This takes the form of a set $\{\psi_{i,0}\}_{i=1}^N$.
2. Using these eigenvectors/eigenfunctions as a basis, we can approximate the solutions to our more complicated system, $H_0 + \delta$. Namely if $(H_0 + \delta)\psi_i = E_i\psi_i$, then $\psi_i = \sum_{j=1}^N c_j\psi_{j,0}$.

We will treat electron-electron interactions as a perturbation on our original system as it yields small effects. To actually utilize perturbation theory, we will use Green's functions which are given by

$$G_0(\omega) = (\omega - H_0)^{-1} \tag{3.9}$$

where H_0 is our unperturbed Kohn-Sham Hamiltonian (the term in brackets within Eqn. 3.5) and ω is real-valued. Solving this explicitly yields

$$G_0(\mathbf{r}, \mathbf{r}', \omega) = \sum_n \frac{\psi_n(\mathbf{r})\psi_n^*(\mathbf{r}')}{\omega - \epsilon_n + i\eta \operatorname{sgn}(\epsilon_n - E_f)}. \tag{3.10}$$

This has η be some positive-valued infinitesimal value which selects a branch-cut, and E_f is our *Fermi energy*. This is the energy at which a material is charge neutral. We can now define our perturbed (interacting) Hamiltonian,

$$H_0(\mathbf{r}) + \Sigma(\mathbf{r}, \mathbf{r}', \omega) = H(\mathbf{r}, \mathbf{r}', \omega) \quad (3.11)$$

where Σ represents our electron-electron interactions (we will solve for this soon). Finding the Green's function for our interacting Hamiltonian, $G(\mathbf{r}, \mathbf{r}', \omega)$,

$$(H_0 - \omega) + \Sigma = H - \omega \implies G^{-1} = G_0^{-1} - \Sigma \quad (3.12)$$

$$\implies G = G_0 + G_0 \Sigma G \quad (3.13)$$

where this final result is known as the *Dyson equation*. Henceforth, it is helpful to view these Green's functions as propagators for the electrons in question. Also note our units, where ω and Σ both must be in units of energy.

3.3.2 Screened Coulomb interactions

We will now investigate more into Σ and how it relates to perturbation theory. To do so, we can write this self-interaction using Feynman diagrams such that we have one incoming propagator and one outgoing propagator. This makes sense intuitively as we are working within the one-electron picture. Of particular interest are diagrams that are easiest to solve, this is shown in Figure 3.1 and is called the Random Phase Approximation (RPA).

These specific interactions are called *screened Coulomb interactions*, where we denote their sum as W . First let $\nu := e^2/|\mathbf{r}_i - \mathbf{r}_j|$. Thanks to efforts by Adler and Wiser, we can analytically solve for χ_0 which denotes the creation/annihilation of new self-interacting particles. Let our first vertex be denoted by (\mathbf{r}_1, t_1) and our second vertex by (\mathbf{r}_2, t_2) , where our new particles are given by ψ_a (virtual) and ψ_b (occupied). This yields

$$\chi_0(\mathbf{r}_1, \mathbf{r}_2, \omega) = \sum_b^{\text{occ.}} \sum_a^{\text{virt.}} \frac{\langle \psi_a | \mathbf{r}_1 | \psi_b \rangle \langle \psi_b | \mathbf{r}_2 | \psi_a \rangle}{\epsilon_b - \epsilon_a - \omega} + \sum_b^{\text{occ.}} \sum_a^{\text{virt.}} \frac{\langle \psi_b | \mathbf{r}_1 | \psi_a \rangle \langle \psi_a | \mathbf{r}_2 | \psi_b \rangle}{\epsilon_a - \epsilon_b - \omega}. \quad (3.14)$$

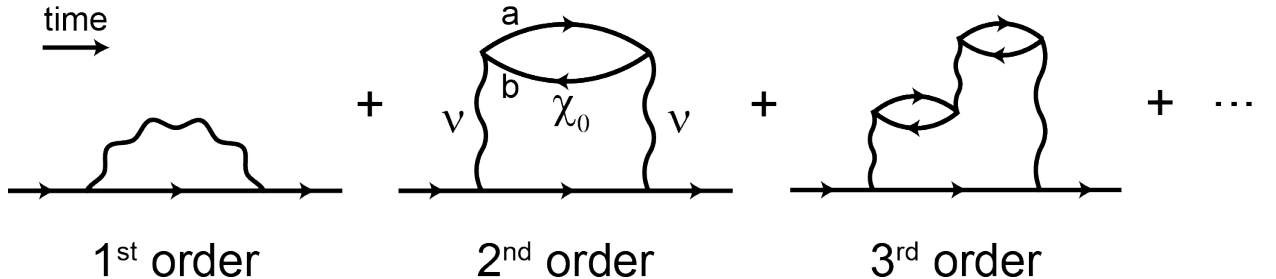


Figure 3.1: Feynman diagrams representing our screened Coulomb interactions up to third order. Note our creation and annihilation loops are denoted by χ_0 and bounded by ν 's, which are both defined in the text. a and b are used for labels on our new virtual (ψ_a) and occupied (ψ_b) states.

Writing this expression in terms of our Green's function yields

$$\chi_0(\mathbf{r}_1, t_1, \mathbf{r}_2, t_2) = -G_0(\mathbf{r}_1, t_1, \mathbf{r}_2, t_2)G_0(\mathbf{r}_2, t_2, \mathbf{r}_1, t_1). \quad (3.15)$$

If we now sum over all screened interactions (outlined in Figure 3.1), it turns into a geometric series given by

$$W = \nu + \nu\chi_0\nu + \nu\chi_0\nu\chi_0\nu + \dots = \nu(1 - \chi_0\nu)^{-1}. \quad (3.16)$$

For compactness, let $\epsilon^{-1} := (1 - \chi_0\nu)^{-1}$. Thus we now have an analytical expression for the screened Coulomb interactions:

$$W(\mathbf{r}, \mathbf{r}', \omega) = \frac{e^2 \epsilon^{-1}(\mathbf{r}, \mathbf{r}', \omega)}{|\mathbf{r} - \mathbf{r}'|}. \quad (3.17)$$

3.3.3 GW approximations

We now have the necessary pieces to take into account our electron-electron interactions. From a perturbation on our original Kohn-Sham Hamiltonian in Eqn. 3.5, we can integrate these new interactions over all space to get our *quasi-particle equation*:

$$\begin{aligned} \left[-\frac{\hbar^2}{2m_e} \nabla^2 + V(\mathbf{r}) + \int d\mathbf{r}' \frac{\rho(\mathbf{r}')}{|\mathbf{r} - \mathbf{r}'|} + V_{XC}(\mathbf{r}) \right] \psi_i(\mathbf{r}) \\ + \int d\mathbf{r}' \Sigma(\mathbf{r}, \mathbf{r}', E_i) \psi_i(\mathbf{r}') = E_i \psi_i(\mathbf{r}) \end{aligned} \quad (3.18)$$

where $\Sigma := iGW$ as defined in Equations 3.13 and 3.17. Explicitly, this is given by

$$\begin{aligned} \Sigma(\mathbf{r}, \mathbf{r}', E) = \frac{i}{2\pi} \int_{-\infty}^{+\infty} d\omega \sum_n^{\text{all}} \frac{\psi_n(\mathbf{r})\psi_n^*(\mathbf{r}')}{\omega - E - E_n + i\eta \operatorname{sgn}(E_n - E_f)} \\ \times e^2 \int d\mathbf{r}'' \frac{\epsilon^{-1}(\mathbf{r}, \mathbf{r}'', \omega)}{|\mathbf{r}'' - \mathbf{r}'|}. \end{aligned} \quad (3.19)$$

The difficulty now lies in solving this much more complicated expression. We perform the simplest form of this calculation in Section 5.1.2 called a *single shot GW approximation* (G_0W_0). This process first calculates the eigenpairs $\{(\epsilon_i, \psi_i)\}_{i=1}^N$ of the Kohn-Sham Hamiltonian, then $\Sigma = G_0W_0$ from these eigenpairs. We then determine the first-order change in our energy eigenvalues, evaluated by

$$E_i = \epsilon_i + Z_i \cdot \operatorname{Re} \left[\langle \psi_i | -\frac{\hbar^2}{2m_e} \nabla^2 + V(\mathbf{r}) + \int d\mathbf{r}' \frac{\rho(\mathbf{r}')}{|\mathbf{r} - \mathbf{r}'|} + \Sigma(\epsilon_i) | \psi_i \rangle - \epsilon_i \right] \quad (3.20)$$

where

$$Z_i := \left(1 - \langle \psi_i | \frac{\partial \Sigma(\omega)}{\partial \omega} \Big|_{\omega=E_i} | \psi_i \rangle \right)^{-1}. \quad (3.21)$$

Chapter 4

Structural determination and analysis

4.1 Atomistic structure

To determine the atomistic structure, I started with an initial guess provided by Dr. Shiva Poudel. We then used the VASP code package [29, 30, 31, 32] with generalized gradient approximation (GGA) pseudopotentials [33]. This utilized opt-PBE GGA exchange-functionals and accounted for extra van der Waals (vdW) forces [34, 35]. Within VASP, we used two separate algorithms to determine the atomistic structure with the minimum energy (and with the minimum forces acting upon its atoms):

1. Conjugate gradient method: Ions, and other degrees-of-freedom, are relaxed along the line pointing along the energy's steepest descent. This is good when our initial guess is not great (IBRION = 2).
2. Quasi-Newton algorithm (RMM-DIIS): This uses the forces/force tensor to determine a search direction on our atoms. It converges quickly for good initial guesses, so we used this once we had a more accurate guess from the prior algorithm (IBRION = 1).

Through these algorithms, we determined our in-plane lattice vectors ($\mathbf{a}_1, \mathbf{a}_2$). Our out-of-plane lattice vector (\mathbf{a}_3) was set to have 9 \AA of vacuum above and below our monolayer. This is to avoid interactions between repeated structures within VASP. All lattice vectors are in angstroms (\AA)

$$\mathbf{a}_1 = \begin{pmatrix} 4.330319405 \\ 0 \\ 0 \end{pmatrix} \quad \mathbf{a}_2 = \begin{pmatrix} 0 \\ 4.076563835 \\ 0 \end{pmatrix} \quad \mathbf{a}_3 = \begin{pmatrix} 0 \\ 0 \\ 20.950189870 \end{pmatrix}. \quad (4.1)$$

This unit cell holds four atoms: two Sn atoms and two S atoms. Their locations are reported in Table 4.1 and shown pictorially within Figure 4.1. This structure is denoted a *buckled honeycomb lattice*, where its intrinsic polarization points *in-plane along the armchair direction* [12]. The lack of inversion symmetry for this structure is verified through the algorithm discussed in Section 4.4.

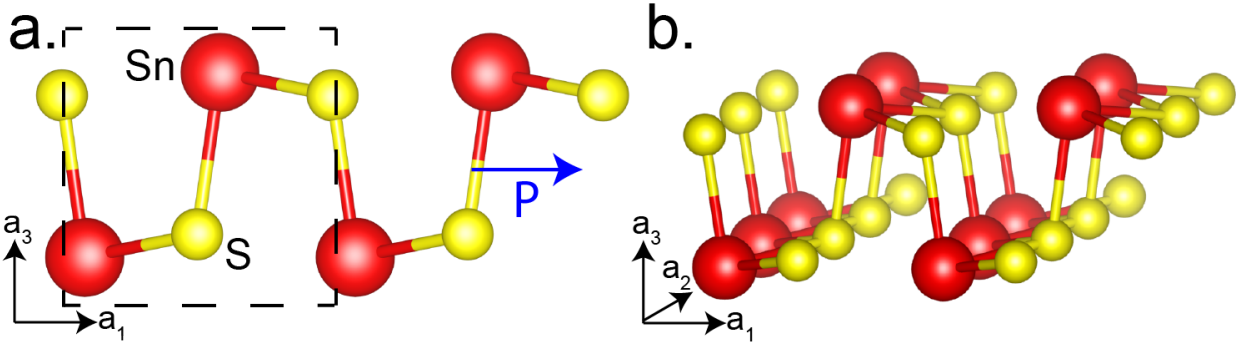


Figure 4.1: Atomistic structure of a SnS monolayer. (a) The in-plane view includes a dashed-boxed showing our rectangular unit cell and a blue arrow showing the direction of our intrinsic polarization (P). (b) Another view showing periodicity along \mathbf{a}_2 is also provided.

4.2 Symmetry analysis

Recall that a group is an ordered pair (G, \star) where G is a non-empty set and $\star : G \times G \rightarrow G$ is a binary operation such that

1. There exists a unique identity element: for all $g \in G$, there exists some unique $e \in G$ such that $g \star e = e \star g = g$.
2. For each element, there exists a unique inverse element: for each $g \in G$, there exists some unique $g^{-1} \in G$ such that $g \star g^{-1} = g^{-1} \star g = e$.
3. Elements are associative on (\star) : for any $g_1, g_2, g_3 \in G$, $(g_1 \star g_2) \star g_3 = g_1 \star (g_2 \star g_3)$.

SnS and other group-IV monochalcogenides (excluding lead-based materials, PbX) belong to the $P2_1mn$ space group [12]. The elements of this group are symmetry operations which leave our crystal structure unchanged.

4.3 Matrix representation

Given an atomic location at $(x, y, z)^T_d \in \mathbb{R}^3$, we will first expand this into four dimensions as $\mathbf{r} = (x, y, z, 1)^T$. This new dimension allows us to perform rigid translations through

	Cartesian			Direct		
	x (\AA)	y (\AA)	z (\AA)	\mathbf{a}_1	\mathbf{a}_2	\mathbf{a}_3
Sn	0.36501	0.00000	9.00000	0.08429	0.00000	0.42959
Sn	2.53017	2.03828	11.9502	0.58429	0.50000	0.57041
S	2.16525	2.03828	9.36562	0.50002	0.50000	0.44704
S	0.00009	0.00000	11.5846	0.00005	0.00000	0.55296

Table 4.1: Atomistic locations of our tin and sulfur atoms within the unit cell defined in Eqn 4.1.

matrix multiplication. Our space group elements then take the form of real (4×4) matrices: $P2_1mn = \{M_1, M_2, M_3, M_4\}$. Explicitly, these matrices are

$$M_1 = \begin{pmatrix} 1 & 0 & 0 & 0 \\ 0 & 1 & 0 & 0 \\ 0 & 0 & 1 & 0 \\ 0 & 0 & 0 & 1 \end{pmatrix} \quad (4.2)$$

$$M_2 = \begin{pmatrix} 1 & 0 & 0 & 1/2 \\ 0 & -1 & 0 & 1/2 \\ 0 & 0 & -1 & 0 \\ 0 & 0 & 0 & 1 \end{pmatrix} \quad (4.3)$$

$$M_3 = \begin{pmatrix} 1 & 0 & 0 & 0 \\ 0 & -1 & 0 & 0 \\ 0 & 0 & 1 & 0 \\ 0 & 0 & 0 & 1 \end{pmatrix} \quad (4.4)$$

$$M_4 = \begin{pmatrix} 1 & 0 & 0 & 1/2 \\ 0 & 1 & 0 & 1/2 \\ 0 & 0 & -1 & 0 \\ 0 & 0 & 0 & 1 \end{pmatrix}. \quad (4.5)$$

Geometrically, this corresponds to: M_1 is the identity, M_2 is a 180° rotation about \mathbf{a}_1 with a translation of $(1/2, 1/2, 0)_d$, M_3 is a reflection across the $\mathbf{a}_1\mathbf{a}_3$ plane, and M_4 is a reflection across the $\mathbf{a}_1\mathbf{a}_2$ plane with a translation along $(1/2, 1/2, 0)_d$. Table 4.2 shows how our group is closed under applying these operations.

	1	2	3	4
1	1	2	3	4
2	2	1	4	3
3	3	4	1	2
4	4	3	2	1

Table 4.2: Multiplication table for space group $P2_1mn$. Note that each entry value i corresponds to our matrix M_i . For ordering, each element is calculated by $(row) \times (col)$. This also shows $P2_1mn$ is an abelian group, where $M_iM_j = M_jM_i$ for $i, j \in \{1, 2, 3, 4\}$.

4.4 Algorithm to check for inversion symmetry

For this project, and subsequent ones as well, we need to verify that our relaxed structure is *non-centrosymmetric*. Note this is shown explicitly within the previous section, where the inversion operator is not an element of our group. Nevertheless, my algorithm checks this and allows for easier checking for new materials where one may not know the space group.

We start with a known unit cell with a variable number of atomic species. Formatting-wise, the algorithm inputs a POSCAR file from any VASP calculation. Now pick the elemental

species with the *least* number of atoms and call this species L . As our unit cell ($\mathbf{a}_1, \mathbf{a}_2, \mathbf{a}_3$) spans the material, we can first assume that if our inversion point exists, it must lie within our unit cell. If it exists, then it must lie at a midpoint between atoms of the same atomic species. To check all possibilities, we will find our midpoints between L atoms in a central unit cell and L atoms on a $3 \times 3 (\times 3)$ supercell for a slab(bulk) material.

We now have a list of potential inversion points. We pick one and invert all atoms in the unit cell through it. Explicitly, if our atom is at $\mathbf{r} = (x, y, z)_d$ and we invert it through $\mathbf{P} = (P_x, P_y, P_z)$, we get a new vector $\mathbf{r}' = (x', y', z')_d$ defined as

$$\mathbf{r}' := 2\mathbf{P} - \mathbf{r}. \quad (4.6)$$

Quickly showing why this transformation works, we will use matrix multiplication. First, we will translate our system such that \mathbf{P} is at the origin, reflect through the origin, then translate our system back. Putting these transformations into one matrix yields

$$\begin{pmatrix} 1 & 0 & 0 & P_x \\ 0 & 1 & 0 & P_y \\ 0 & 0 & 1 & P_z \\ 0 & 0 & 0 & 1 \end{pmatrix} \begin{pmatrix} -1 & 0 & 0 & 0 \\ 0 & -1 & 0 & 0 \\ 0 & 0 & -1 & 0 \\ 0 & 0 & 0 & 1 \end{pmatrix} \begin{pmatrix} 1 & 0 & 0 & -P_x \\ 0 & 1 & 0 & -P_y \\ 0 & 0 & 1 & -P_z \\ 0 & 0 & 0 & 1 \end{pmatrix} = \begin{pmatrix} -1 & 0 & 0 & 2P_x \\ 0 & -1 & 0 & 2P_y \\ 0 & 0 & -1 & 2P_z \\ 0 & 0 & 0 & 1 \end{pmatrix}. \quad (4.7)$$

Applying this to our vector \mathbf{r} yields

$$\begin{pmatrix} x' \\ y' \\ z' \\ 1 \end{pmatrix} = \begin{pmatrix} -1 & 0 & 0 & 2P_x \\ 0 & -1 & 0 & 2P_y \\ 0 & 0 & -1 & 2P_z \\ 0 & 0 & 0 & 1 \end{pmatrix} \begin{pmatrix} x \\ y \\ z \\ 1 \end{pmatrix} = \begin{pmatrix} -x + 2P_x \\ -y + 2P_y \\ -z + 2P_z \\ 1 \end{pmatrix}. \quad (4.8)$$

To see if this is truly an inversion point, we simply check if \mathbf{r}' points to another atom of the same species. If this is satisfied for all atoms in the unit cell (given some defined convergence criterion), we have found an inversion point. If this is *not* satisfied for all atoms in the unit cell, we check the next possible inversion point until we run out. A schematic of this is shown in Figure 4.2. If the material is inversion symmetric, it creates an output file; this contains data on where our inversion point(s) maps atoms within the unit cell. That helps for double-checking results and preventing false positives stemming from a large convergence criterion.

This code is given in Appendix A.

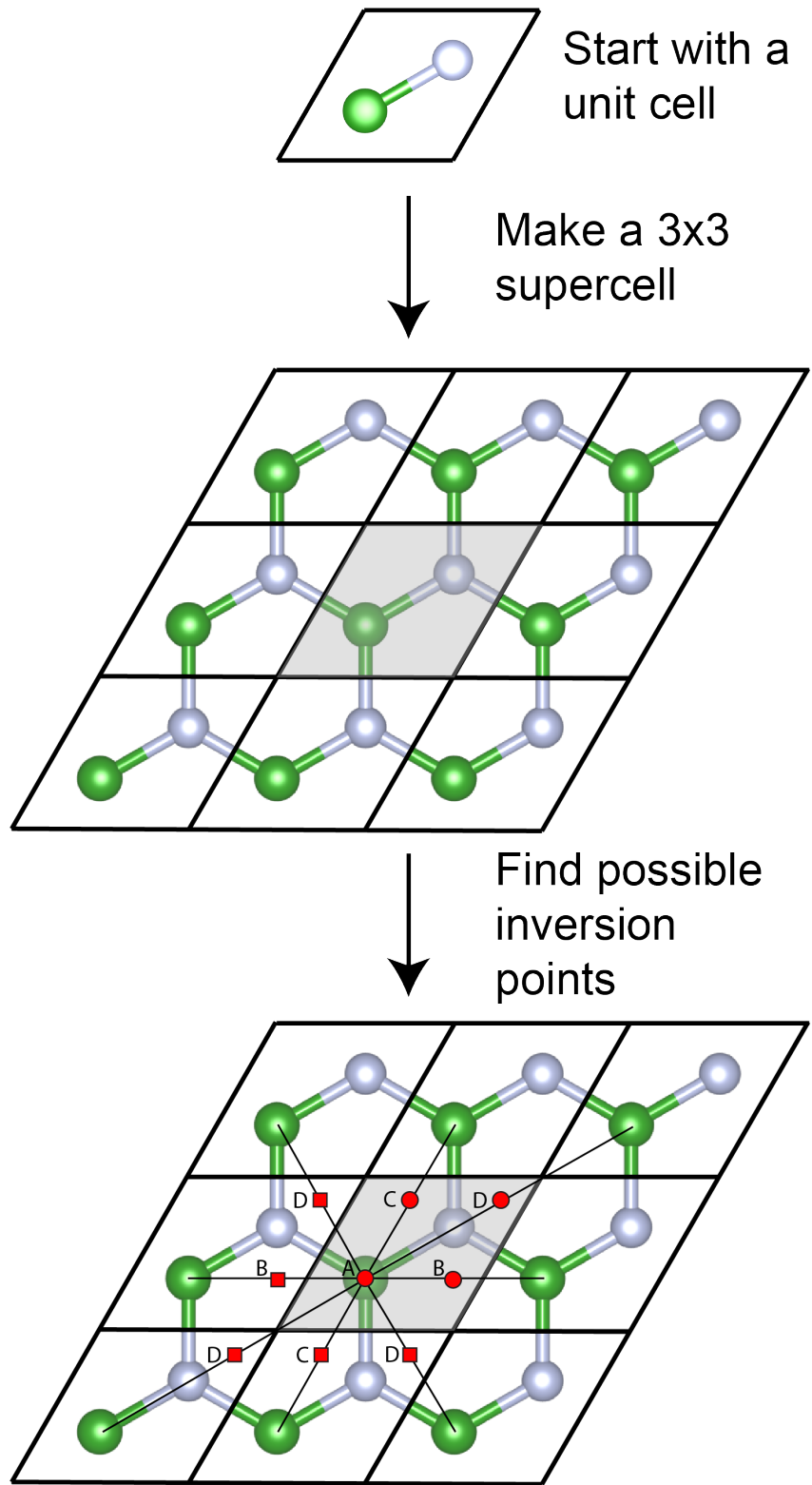


Figure 4.2: Inversion point checking algorithm, applied to hexagonal boron nitride (hBN). Green dots are boron, and gray dots are nitrogen. Possible inversion points are shown in red. The squares are degenerate points and are not considered. Note none of the circles work, as hBN is noncentrosymmetric.

Chapter 5

Calculating the electronic structure

When analyzing a material, it is important to see how its electrons behave. As such, I calculated the electronic structure of the SnS monolayer. Given some momentum \mathbf{k} , this shows the possible energy (eigen)values for our electrons. For a fixed \mathbf{k} , these energies are quantized as a result of solving the Schrödinger equation of Section 3.1. Henceforth, we will use reciprocal space within calculations. Briefly, our reciprocal lattice vectors (in reciprocal/momentum space) are defined as

$$\mathbf{b}_1 = \frac{2\pi}{\Omega}(\mathbf{a}_2 \times \mathbf{a}_3) \quad \mathbf{b}_2 = \frac{2\pi}{\Omega}(\mathbf{a}_3 \times \mathbf{a}_1) \quad \mathbf{b}_3 = \frac{2\pi}{\Omega}(\mathbf{a}_1 \times \mathbf{a}_2) \quad (5.1)$$

such that $\Omega := \mathbf{a}_1 \cdot (\mathbf{a}_2 \times \mathbf{a}_3)$ is the unit cell volume and $\mathbf{a}_i \cdot \mathbf{b}_j = 2\pi\delta_{ij}$, where $i, j \in \{1, 2, 3\}$ and δ_{ij} is the Kronecker delta.

5.1 Plane wave basis

5.1.1 Without GW approximations

We first calculated the electronic structure using a plane wave basis in VASP *without* electron-electron interactions. As such, I performed a self-consistent calculation to determine the electron charge distribution and the Fermi energy (E_f , the energy where our material is charge neutral). This used a Monkhorst-Pack k-point mesh containing $18 \times 18 \times 1$ points [36]; anything larger than 1 in this last dimension will have VASP calculate interlayer interactions, which are negligible as we have sufficiently large vacuum above and below the slab. This resulted in our charge distribution shown in Figure 5.1.

Using this data, I used VASP to calculate the Kohn-Sham eigenvalues (Eqn. 3.5) for the $\Gamma - X - S - Y - \Gamma$ k-point path as defined in Table 5.1. For 51 k-points along each path, we can see the electronic structure given in Figure 5.2. See the energy gap, called the band gap, in the middle of our figure; so SnS monolayers are semiconductors. Note the maximum of the bottom (valence) bands and the minimum of the upper (conduction) bands do not occur for the same wavevector \mathbf{k} . Therefore we have an *indirect* band gap of $E_g = 1.612$ eV. This means if an electron is to be excited to the conduction band with the minimum energy, it must pair with lattice vibrations to change its momentum. Another feature is how our bands

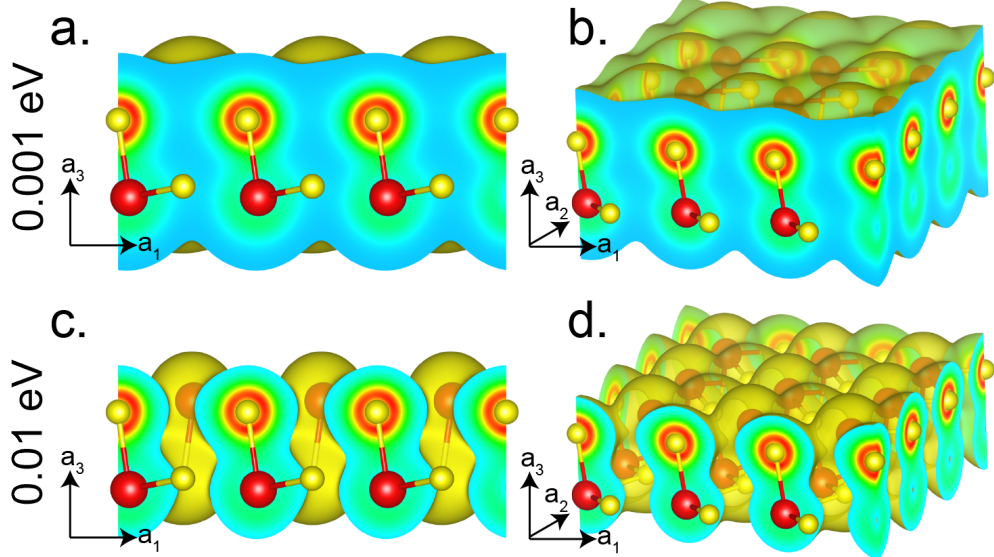


Figure 5.1: Charge (electron cloud) distribution for a SnS monolayer. This plots the energy isosurface for $E = 0.001 \text{ eV}$ (a,b) and for $E = 0.01 \text{ eV}$ (c,d).

\mathbf{k} -point	Cartesian	Direct
Γ	$0\mathbf{b}_1 + 0\mathbf{b}_2 + 0\mathbf{b}_3$	(0,0,0)
X	$(1/2)\mathbf{b}_1 + 0\mathbf{b}_2 + 0\mathbf{b}_3$	(1/2,0,0)
S	$(1/2)\mathbf{b}_1 + (1/2)\mathbf{b}_2 + 0\mathbf{b}_3$	(1/2,1/2,0)
Y	$0\mathbf{b}_1 + (1/2)\mathbf{b}_2 + 0\mathbf{b}_3$	(0,1/2,0)

Table 5.1: High symmetry points of interest within reciprocal space.

become degenerate on the Brillouin zone boundary: $X - S - Y$. In future studies, it would be important to see if these degeneracies are broken when taking into account interactions between the electrons' spin- and orbit-angular momentum (spin-orbit coupling).

Recall that DFT calculations typically minimize our energy functional *without electron-electron interactions*. This approximation manifests in underestimating the bandgap E_g . As incident light will interact with electrons near this energy level, E_g must be more accurate. We will fix this error in Section 5.1.2.

As stated above, we calculated possible energy values for our electrons. But these electrons must be within some (possibly hybridized) orbital. Analyzing this more carefully, we can determine the orbital character as shown in Figure 5.3. These band decompositions take the form of $|\langle Y_{lm}^\alpha | \phi_{n,\mathbf{k}} \rangle|$ which projects our wavefunction $|\phi_{n,\mathbf{k}}\rangle$ onto a given spherical harmonic $|Y_{lm}^\alpha\rangle$. This decomposition will become increasingly important when dealing with numerical atomic orbitals in Section 5.2; we will form our Hamiltonian from these orbitals explicitly. As expected from energies in the periodic table, $E(s) < E(p) < E(d)$ generally. Figure 5.3 also reveals that our indirect band gap must excite an electron such that $|p_x\rangle^S \rightarrow |p_z\rangle^{S_n}$.

5.1.2 With GW approximations

In this section, we finally take into account electron-electron interactions. To do so, we will perform a so-called (*single-shot*) *GW*-approximation. This process is explained in greater detail in Section 3.3.3. One thing to note about VASP’s *GW* implementation is that it relies on an additional basis set. VASP uses plane waves, but this process utilizes *wannier functions* as implemented within Wannier90 (another DFT code) [37]. This was not explained in Section 3.2 as it is a small step within this process. To perform this *GW* calculation using VASP, there are five steps:

1. VASP: Self-consistent calculation (1)
2. VASP: Self-consistent calculation (2)
3. VASP and Wannier90: *GW* calculation
4. Wannier90: Self-consistent calculation
5. Wannier90: Electronic band structure calculation.

Results of this process are shown in Figure 5.4 where we calculated a new electronic band-structure for a SnS monolayer. One may notice that this is *very* similar to our electronic band structure using a standard plane wave basis in Figure 5.2. The crucial difference is the band gap. In changing from a non-*GW* calculation to a *GW* calculation, we have *increased* our band gap from 1.612 eV to 2.016 eV. This is consistent with other group-IV monochalcogenides (GeSe [38] and SnSe [39]), which have band gap increases of the same order when

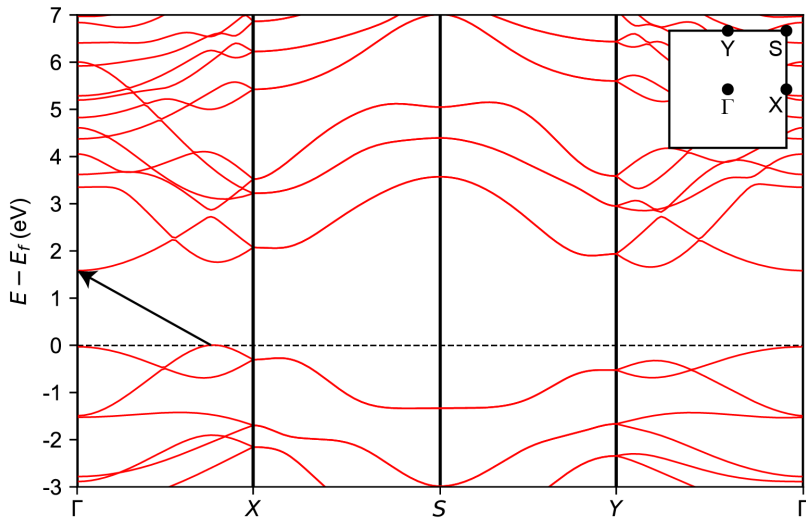


Figure 5.2: Electronic band structure for a SnS monolayer. Our Brillouin zone and high symmetry points are shown pictorially in the inset and defined in Table 5.1.

comparing the two calculations.

Correcting this band gap is the entire reason for taking into account electron-electron interactions, as researchers noticed that DFT band gaps were under-predicting experimental results. The main drawback of this process is that it is very memory intensive. Since the most important difference is an increased band gap, we can instead perform a *scissor operation*, \mathbb{X} . This adds constants to our energy eigenvalues while leaving eigenvectors/eigenfunctions fixed. For our purposes, we can increase our band gaps by using \mathbb{X} to slightly increase all energies greater than the Fermi energy. Of course, this assumes we already know our increased

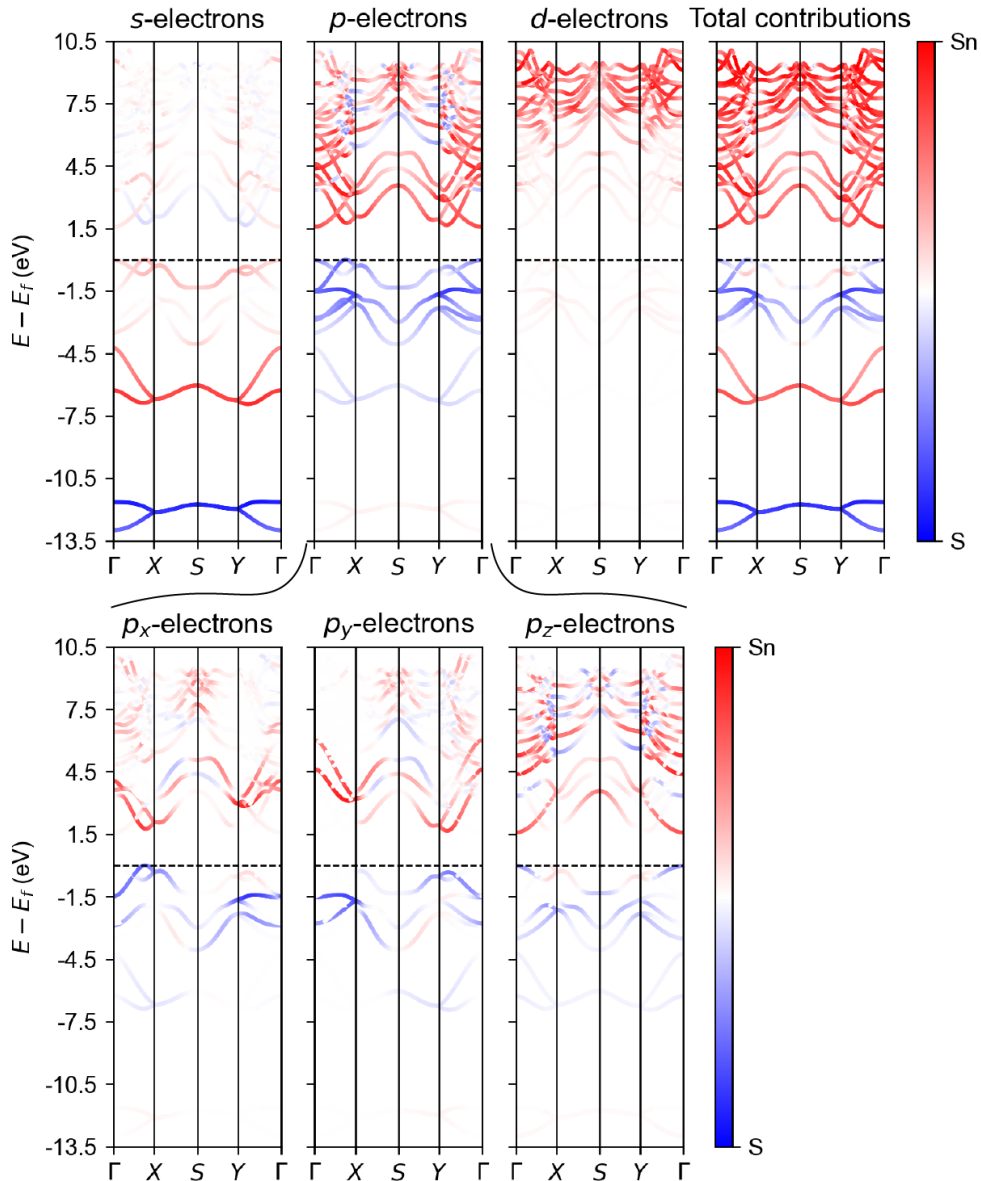


Figure 5.3: Orbital decomposition of SnS energy bands. This shows which energy regions correspond to which orbital/atom.

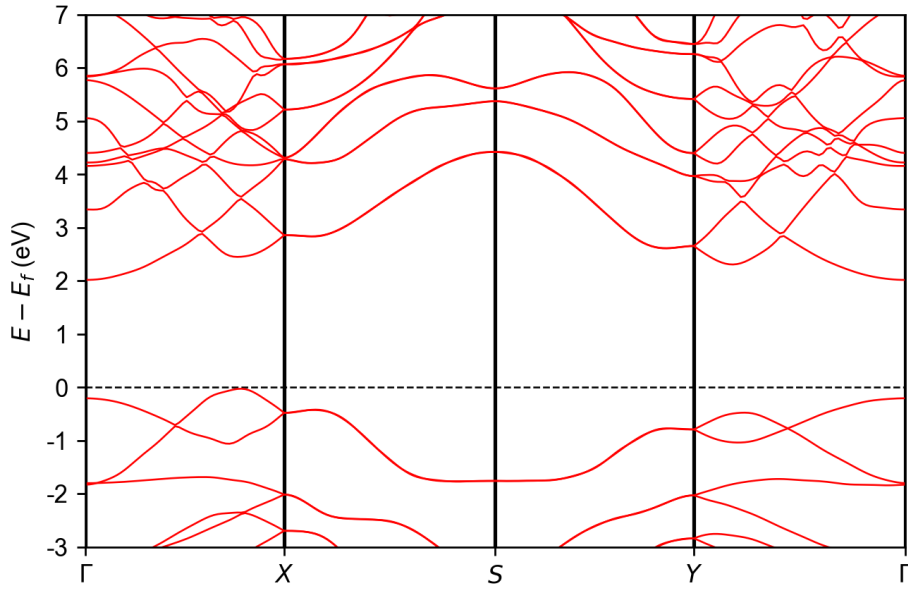


Figure 5.4: Electronic band structure for a SnS monolayer from a single shot GW approximation (G_0W_0). This takes into account electron-electron interactions, leading to a more accurate band gap.

band gap, which could be experimentally determined.

Writing \mathbb{X} in a matrix representation, assume that we have a system satisfying $H\psi_i = E_i S \psi_i$ such that $1 \leq i \leq N$. Namely, we are interested in the eigenpairs of H with respect to S . As we are working with matrices, this is expressed as

$$H = SP\Lambda P^{-1} \quad (5.2)$$

where

$$P = \begin{pmatrix} | & & | \\ \psi_1 & \dots & \psi_N \\ | & & | \end{pmatrix} \quad \text{and} \quad (\Lambda)_{ij} = \begin{cases} E_i & : i = j \\ 0 & : \text{else} \end{cases}. \quad (5.3)$$

Recall that we are modeling a physical system where all energies are real-valued (with no imaginary components). This is true if and only if H and S are both Hermitian, so $H = H^\dagger$ and $S = S^\dagger$. This implies that our eigenvectors are real-valued and orthogonal, so $P^{-1} = P^T = P^\dagger$. Therefore $H = SP\Lambda P^\dagger$.

While our earlier expressions set S to the identity matrix, we will keep everything general to help in our discussions on numerical atomic orbitals in Sections 5.2 and 6. Now let $I \subseteq \{1, \dots, N\}$ be a subset of indices for our eigenvalues, where we want to add δ_i to the $I \ni i$ -th eigenvalue. Then our operation takes the form:

$$\mathbb{X} := SP\Delta P^\dagger \quad \text{where} \quad (\Delta)_{ij} := \begin{cases} \delta_i & : i = j \\ 0 & : \text{else} \end{cases}. \quad (5.4)$$

To actually use this operation (shifting certain eigenvalues while leaving eigenvectors/eigenfunctions constant) we simply find the eigenpairs of $(H + \mathbb{X})$ with respect to S . Quickly justifying this, finding these eigenpairs results in

$$H + \mathbb{X} = SP\Lambda P^\dagger + SP\Delta P^\dagger = SP(\Lambda + \Delta)P^\dagger. \quad (5.5)$$

Note that our original eigenvectors, stored in P , remain the same while our diagonal matrix, in parenthesis, has been shifted by Δ . Thus we have our desired effect.

5.2 Numerical atomic orbital basis

Another option for our basis set, as discussed in Section 3.2, is numerical atomic orbitals. This defines single-electron orbitals for each atom within our material, such as $|s\rangle$ and $|p\rangle$. This basis is not as accurate as plane waves but allows for cheaper calculations. One consequence of this basis is that interacting orbitals from different atoms are not necessarily orthogonal (as in the case of plane waves). This requires us to rewrite our system more generally as

$$H|\phi_i\rangle = E_i S|\phi_i\rangle \quad (5.6)$$

such that

$$(H)_{ij} = \langle \phi_i | \hat{H} | \phi_j \rangle \quad \text{and} \quad (S)_{ij} = \langle \phi_i | \phi_j \rangle. \quad (5.7)$$

From this definition, we then think of H and S as matrices. Henceforth we will call these Hamiltonian and overlap matrices, respectively. In this representation, each column and row of our matrices corresponds to some orbital (for all atoms in the unit cell). Since our light-matter interactions excite our electrons to high energies, it is essential to include d orbitals. Thus, for each atom, we apply nine orbitals: $s, p_y, p_z, p_x, d_{xy}, d_{yz}, d_{z^2-r^2}, d_{xz}$, and $d_{x^2-y^2}$. As our unit cell has four atoms, we have $4 \times 9 = 36$ resultant energies from our 36×36 system. We utilized SIESTA [40] to find the band structure presented in Figure 5.5. Importantly, see how this data has a band gap of 1.617 eV; this is comparable with our original, non-GW, band gap. Assuming our energy eigenvalues start with $i = 1$ and are increasing, we will apply the scissor operation defined as

$$\mathbb{X} := SP\Delta P^\dagger \quad \text{where} \quad (\Delta)_{ij} := \begin{cases} 0.308\delta_{i,j} & : i > 10 \\ 0 & : \text{else} \end{cases}, \quad (5.8)$$

where $\delta_{i,j}$ is the Kronecker delta, increases this band gap to match that of the GW approximations. Figure 5.6 shows the resultant band structure.

We can also find the orbital decomposition of this band structure, as done in the plane-wave basis in Figure 5.3. Instead of projecting our bands onto spherical harmonics, we can simply exploit the fact that our basis is already atomic orbitals on our different atoms. This means that for some eigenvalue (energy), its corresponding eigenvector contains this decomposition data. So the normalized coefficients squared yield this weight for each orbital. That is shown in Figures 5.7 and 5.8 for SnS using different basis sets. The first uses just s and p orbitals on each atom within the unit cell while the second uses s, p , and d orbitals. We will soon be studying another group-IV monochalcogenide, SnTe, so its band structure for both basis sets is shown in Figures 5.9 and 5.10 respectively.

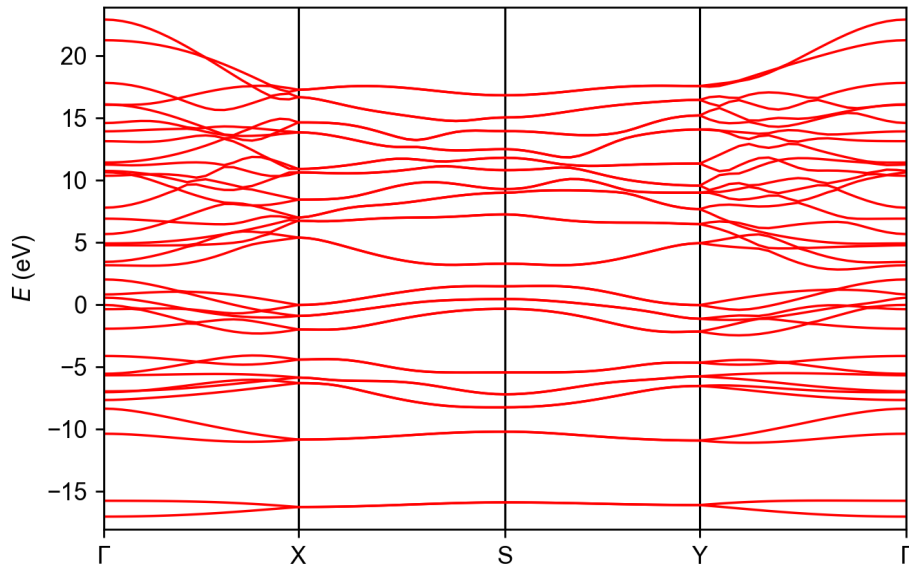


Figure 5.5: Electronic band structure for a SnS monolayer with a numerical atomic orbital basis.

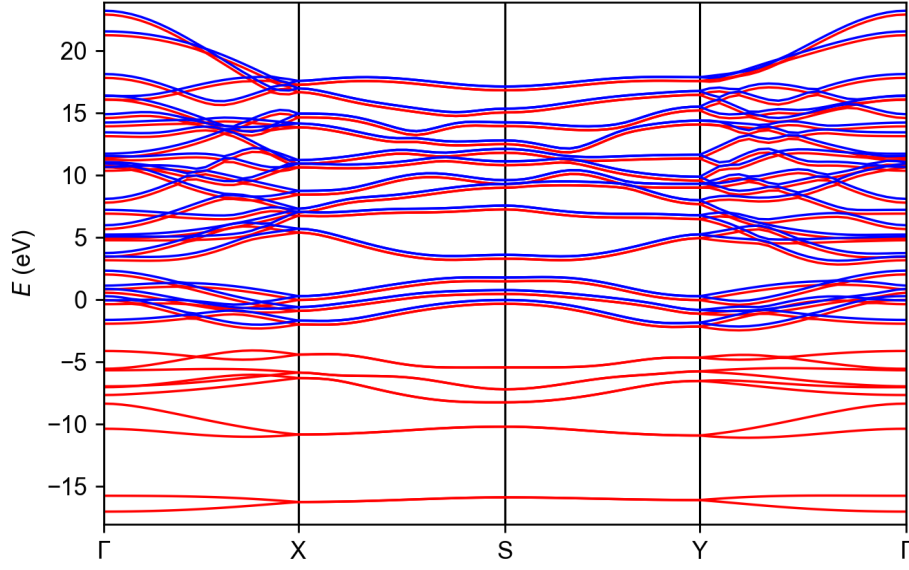


Figure 5.6: Electronic band structure for a SnS monolayer with a numerical atomic orbital basis *applying the scissor operation* defined in Eqn 5.8. Our old bands are in red, then our shifted (conduction) bands are in blue.

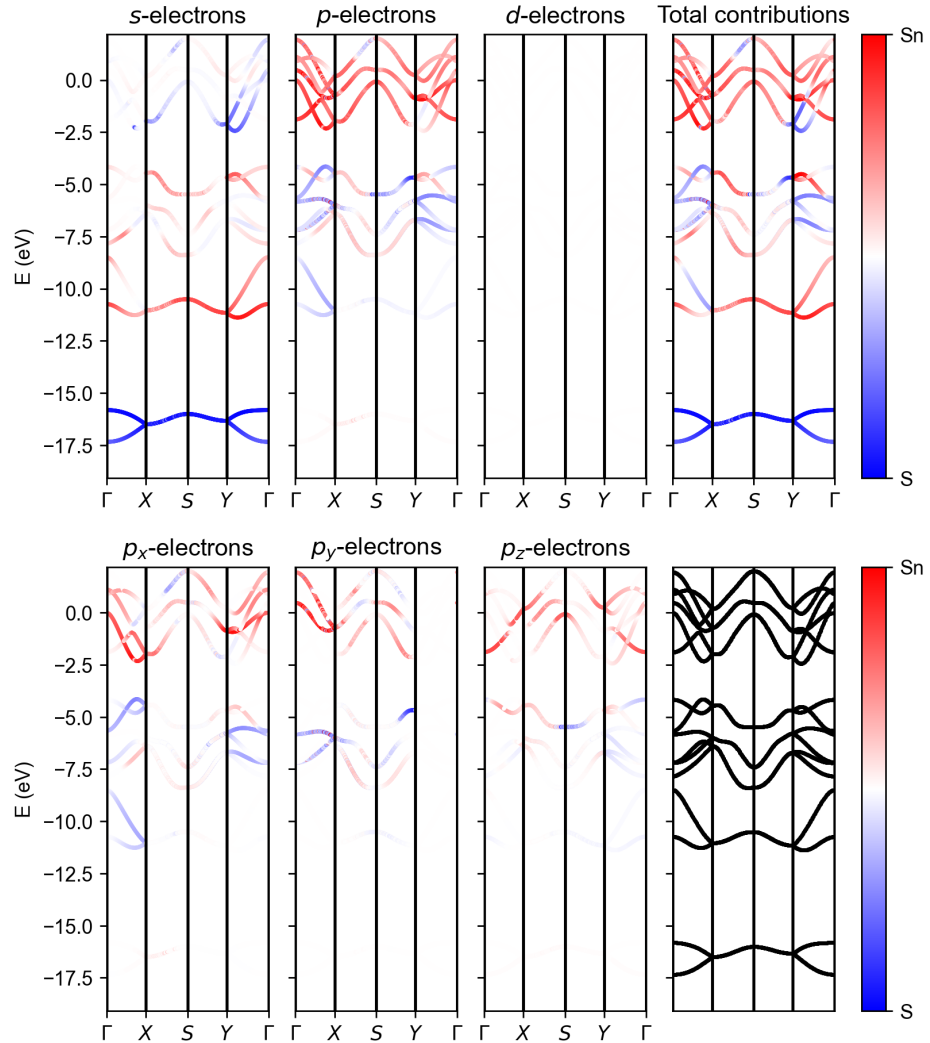


Figure 5.7: Decomposed electronic band structure for a SnS monolayer with a numerical atomic orbital basis of *s* and *p* orbitals.

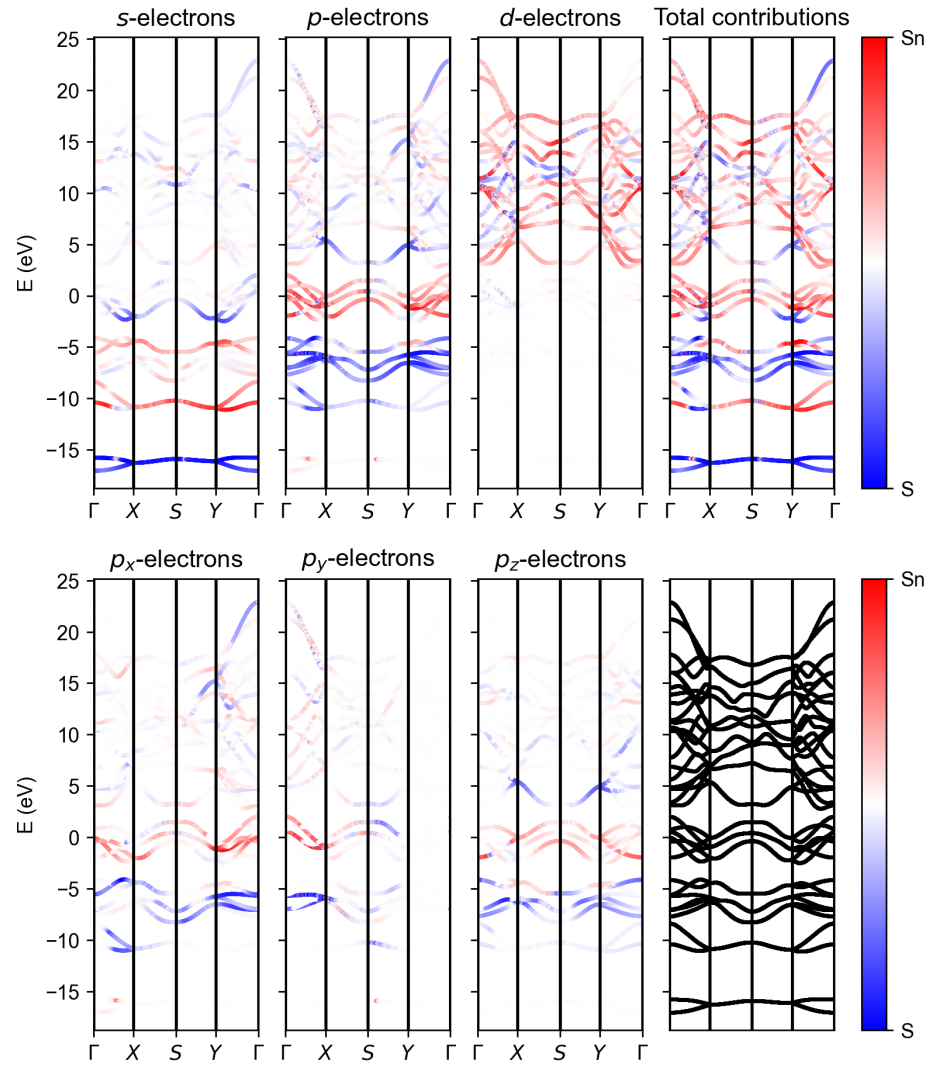


Figure 5.8: Decomposed electronic band structure for a SnS monolayer with a numerical atomic orbital basis of s , p , and d orbitals.

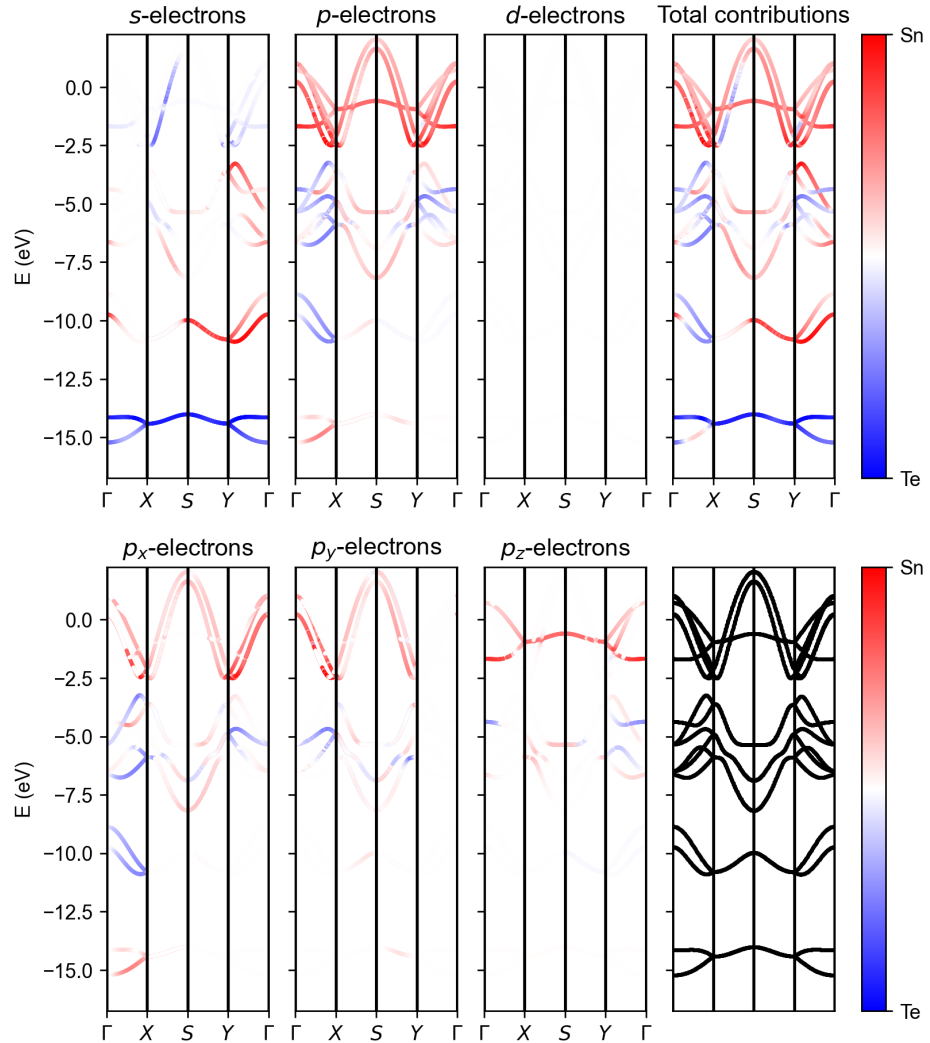


Figure 5.9: Decomposed electronic band structure for a SnTe monolayer with a numerical atomic orbital basis of *s* and *p* orbitals.

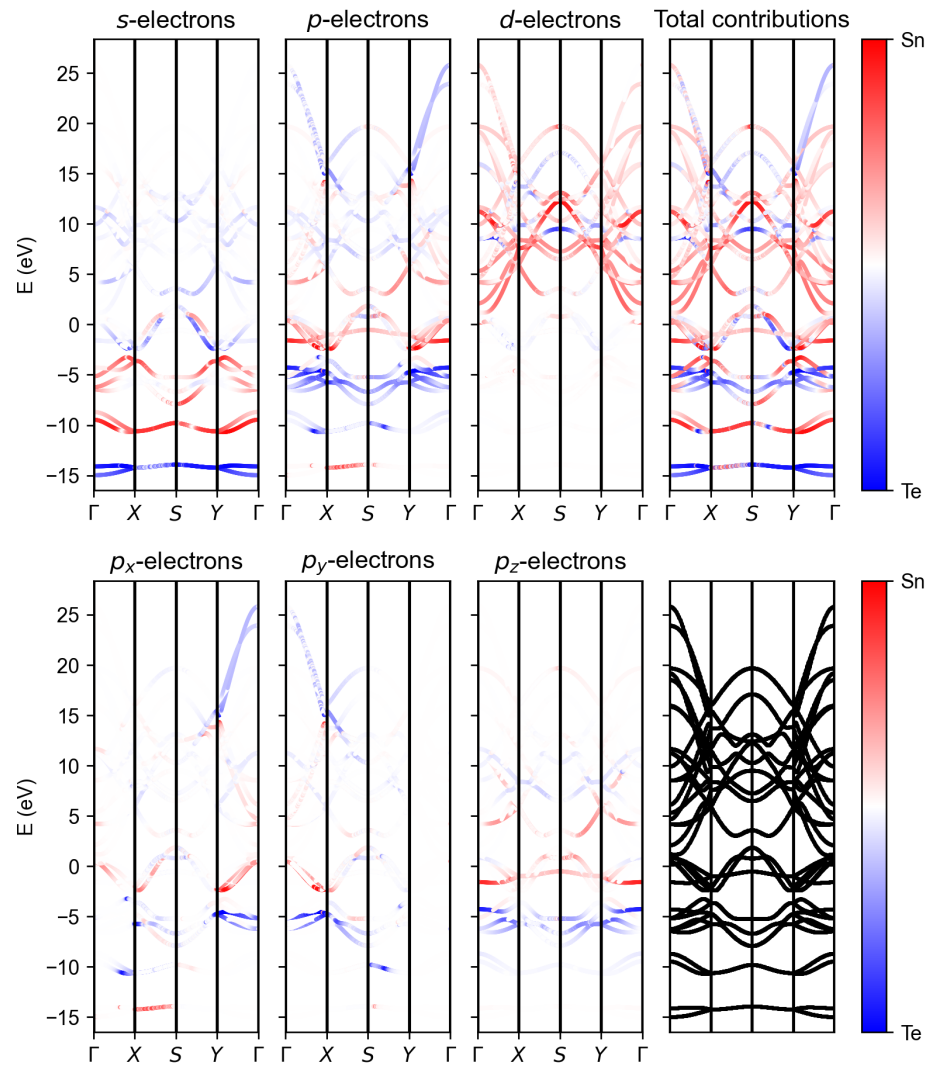


Figure 5.10: Decomposed electronic band structure for a SnTe monolayer with a numerical atomic orbital basis of s , p , and d orbitals.

Chapter 6

Creating a tight-binding representation

6.1 Linear combination of atomic orbitals

In creating a new representation for our physical systems, we will quickly recall our localized atomic orbital bases. This works in a matrix formalism, where each row and column of our matrices corresponds to some orbital on some atom within our unit cell. This must satisfy

$$H|\phi_i\rangle = E_i S|\phi_i\rangle \quad (6.1)$$

such that

$$(H)_{ij} = \langle \phi_i | \hat{H} | \phi_j \rangle \quad \text{and} \quad (S)_{ij} = \langle \phi_i | \phi_j \rangle \quad (6.2)$$

where H and S are our Hamiltonian and overlap matrices. Note this only includes interactions for up to two orbitals (up to 'two-center integrals'). While this makes things less accurate than our typical numerical atomic orbital basis, it allows for significant simplifications and broader applications.

For didactic purposes, let us find a new way to determine the interaction of a $|p_x\rangle$ orbital and a $|p_y\rangle$ orbital on different atoms. This is shown pictorially in Figure 6.1, where our orbitals are displaced by some vector \mathbf{R} in the same plane. We can now 'project' our orbitals onto this displacement vector, where we now have two orthogonal components; one parallel to $\hat{\mathbf{R}}$, called $\hat{\mathbf{R}}$, and one perpendicular to $\hat{\mathbf{R}}$, called $\hat{\mathbf{R}}^\perp$. We will call these decomposed orbitals $|p_i^\sigma\rangle$ and $|p_i^\pi\rangle$ respectively (for σ and π chemical bonds). To do this, we first define $|p_x\rangle := \hat{\mathbf{x}}$ and $|p_y\rangle := \hat{\mathbf{y}}$ where our displacement vector is normalized as $\hat{\mathbf{R}} := \ell\hat{\mathbf{x}} + m\hat{\mathbf{y}}$ and the orthogonal displacement is $\hat{\mathbf{R}}^\perp = m\hat{\mathbf{x}} - \ell\hat{\mathbf{y}}$. To find our parallel and orthogonal components, we will perform vector projections.

$$|p_x\rangle = \left(\frac{\hat{\mathbf{x}} \cdot \hat{\mathbf{R}}}{|\hat{\mathbf{R}}|^2} \right) \hat{\mathbf{R}} + \left(\frac{\hat{\mathbf{x}} \cdot \hat{\mathbf{R}}^\perp}{|\hat{\mathbf{R}}^\perp|^2} \right) \hat{\mathbf{R}}^\perp = (\hat{\mathbf{x}} \cdot \hat{\mathbf{R}})|p_x^\sigma\rangle + (\hat{\mathbf{x}} \cdot \hat{\mathbf{R}}^\perp)|p_x^\pi\rangle = \ell|p_x^\sigma\rangle + m|p_x^\pi\rangle \quad (6.3)$$

$$|p_y\rangle = \left(\frac{\hat{\mathbf{y}} \cdot \hat{\mathbf{R}}}{|\hat{\mathbf{R}}|^2} \right) \hat{\mathbf{R}} + \left(\frac{\hat{\mathbf{y}} \cdot \hat{\mathbf{R}}^\perp}{|\hat{\mathbf{R}}^\perp|^2} \right) \hat{\mathbf{R}}^\perp = (\hat{\mathbf{y}} \cdot \hat{\mathbf{R}})|p_y^\sigma\rangle + (\hat{\mathbf{y}} \cdot \hat{\mathbf{R}}^\perp)|p_y^\pi\rangle = m|p_y^\sigma\rangle - \ell|p_y^\pi\rangle. \quad (6.4)$$

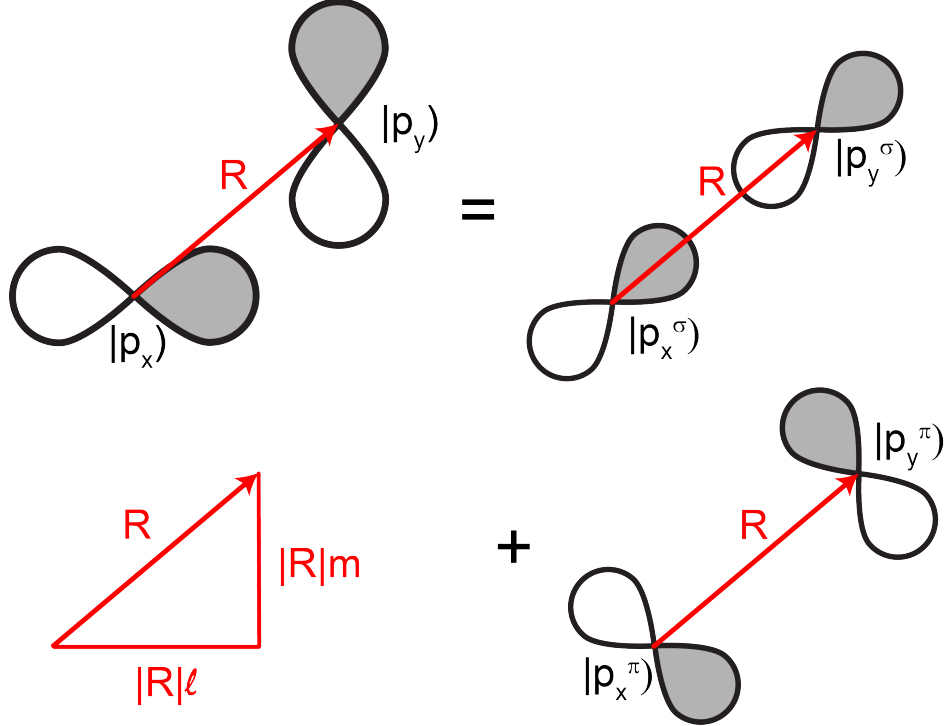


Figure 6.1: Decomposition of two interacting atomic orbitals, namely $|p_x\rangle$ and $|p_y\rangle$, into parallel and orthogonal components. This has our positive lobe shaded in gray and our negative lobe un-shaded (in white).

Because ℓ and m are both real-valued, we can write our desired matrix element as

$$\langle p_x | H | p_y \rangle = (\ell \langle p_x^\sigma | + m \langle p_x^\pi |) H (m |p_y^\sigma \rangle - \ell |p_y^\pi \rangle) \quad (6.5)$$

$$= \ell m \langle p_x^\sigma | H | p_y^\sigma \rangle - \ell^2 \langle p_x^\sigma | H | p_y^\pi \rangle + m^2 \langle p_x^\pi | H | p_y^\sigma \rangle - \ell m \langle p_x^\pi | H | p_y^\pi \rangle. \quad (6.6)$$

By symmetry, we know that our σ bonds don't have a net hopping with our π bonds, implying that

$$\langle p_x | H | p_y \rangle = \ell m V_{pp}^\sigma - \ell m V_{pp}^\pi \quad : \quad V_{pp}^\alpha := \langle p_i^\alpha | H | p_j^\alpha \rangle \quad (6.7)$$

where in this case $\alpha \in \{\sigma, \pi\}$. This expression is shown within Appendix B, along with any possible combination of s , p , and d orbitals, as derived by Slater and Koster using two-center integrals [41]. These are called *projection cosines* and are the basis of our tight-binding (TB) representation. These TB parameters for the Hamiltonian and overlap matrices (V_{ss} , V_{sp} , V_{pp}^σ , V_{pp}^π , ...) can be determined through the .HSX file from a self-consistent SIESTA calculation, where results are shown in Sections 6.1.1-6.1.4. The process of analyzing this data file is surprisingly non-trivial and is outlined in Chapter 7. The code itself is not appended to this document as it is approximately 2500 lines but can be supplied upon request.

This determines all parameters for all possible interactions up to some cut-off where our overlap parameters vanish. The process also assumes that all p orbitals (p_x, p_y, p_z) can be treated equally and that all d orbitals ($d_{xy}, d_{yz}, d_{xz}, d_{x^2-y^2}, d_{z^2-r^2}$) can be treated equally. This is normally a significant approximation but still yields sufficiently accurate results. It

also includes self-interactions called *on-site terms*, where these energies are simply added to our Hamiltonian. Note that the on-site terms for our overlap matrix create the identity matrix. Finally, we also need to know what interaction we are dealing with, whether it is metal-metal (AA), metal-chalcogen (AB), or chalcogen-chalcogen (BB). This interaction data is necessary because, for some interaction radii, there are both AA and BB interactions with different TB parameters.

One thing to note is that $H_{sp} \neq H_{ps}$ for AB interactions. This is because the first term expresses the energy of an electron to hop from $|s\rangle^A \rightarrow |p\rangle^B$ while the second term expresses the energy of an electron to hop from $|p\rangle^A \rightarrow |s\rangle^B$. Thus we also need to satisfy $H_{sp} = H_{ps}$ for both AA and BB interactions.

6.1.1 SnS: single zeta basis

This section reports our onsite Hamiltonian matrix, our tight-binding parameters, and our resultant electronic band structure for a single zeta basis. This basis sets an s , p_y , p_z , and p_x orbital (in this order) on each atom within our unit cell. Our onsite Hamiltonians are given by

$$H_{Sn1-Sn1} = \begin{pmatrix} -10.57775 & 0.00000 & 1.13366 & 0.47252 \\ 0.00000 & -5.24694 & 0.00000 & 0.00000 \\ 1.13366 & 0.00000 & -5.07815 & 0.08462 \\ 0.47252 & 0.00000 & 0.08462 & -5.00002 \end{pmatrix} \quad (6.8)$$

$$H_{Sn2-Sn2} = \begin{pmatrix} -10.57775 & 0.00000 & -1.13367 & 0.47252 \\ 0.00000 & -5.24694 & 0.00000 & 0.00000 \\ -1.13367 & 0.00000 & -5.07815 & -0.08463 \\ 0.47252 & 0.00000 & -0.08463 & -5.00002 \end{pmatrix} \quad (6.9)$$

$$H_{S1-S1} = \begin{pmatrix} -15.61652 & 0.00000 & 0.80422 & -0.51154 \\ 0.00000 & -6.27412 & 0.00000 & 0.00000 \\ 0.80422 & 0.00000 & -6.24413 & -0.24937 \\ -0.51154 & 0.00000 & -0.24937 & -6.18138 \end{pmatrix} \quad (6.10)$$

$$H_{S2-S2} = \begin{pmatrix} -15.61651 & 0.00000 & -0.80423 & -0.51154 \\ 0.00000 & -6.27412 & 0.00000 & 0.00000 \\ -0.80423 & 0.00000 & -6.24411 & 0.24937 \\ -0.51154 & 0.00000 & 0.24937 & -6.18137 \end{pmatrix} \quad (6.11)$$

Distance (\AA)	H_{ss}	H_{sp}	H_{ps}	$H_{pp\sigma}$	$H_{pp\pi}$	Interaction
2.61020	-2.38570	-3.27153	5.61789	3.77419	-1.34659	AB
2.74393	-1.82775	-2.59655	4.77320	3.29312	-1.08703	AB
3.26949	-0.58342	-1.10865	2.29570	2.07673	-0.46353	AB
3.71029	-0.04696	-0.23801	0.23801	0.63863	-0.07199	BB
4.07657	-0.22901	-0.94271	0.94271	1.87122	-0.38036	AA
4.07657	-0.00906	-0.08023	0.08023	0.30474	-0.02975	BB
4.18881	-0.18626	-0.86964	0.86964	1.97265	-0.35409	AA
4.33032	-0.11989	-0.59876	0.59876	1.39527	-0.25224	AA
4.33032	-0.00049	-0.03025	0.03025	0.16148	-0.01386	BB
4.73333	-0.00321	-0.04151	0.10902	0.31100	-0.03059	AB
4.84061	-0.00107	-0.02863	0.08252	0.24923	-0.02078	AB
5.35960	0.00000	-0.00088	0.01147	0.07724	-0.00510	AB
5.94727	-0.00002	-0.00853	0.00853	0.14798	-0.00876	AA
5.94727	0.00010	0.00190	-0.00190	-0.00888	-0.00113	BB
Distance (\AA)	S_{ss}	S_{sp}	S_{ps}	$S_{pp\sigma}$	$S_{pp\pi}$	Interaction
2.61020	0.09135	0.18960	-0.27300	-0.32473	0.10985	AB
2.74393	0.06929	0.15663	-0.23113	-0.30203	0.08921	AB
3.26949	0.01857	0.06043	-0.10428	-0.19122	0.03500	AB
3.71029	0.00037	0.00461	-0.00461	-0.02363	0.00194	BB
4.07657	0.00657	0.04784	-0.04784	-0.15999	0.02303	AA
4.07657	0.00002	0.00088	-0.00088	-0.00772	0.00046	BB
4.18881	0.00457	0.03794	-0.03794	-0.13766	0.01843	AA
4.33032	0.00278	0.02780	-0.02780	-0.11230	0.01375	AA
4.33032	0.00000	0.00018	-0.00018	-0.00300	0.00014	BB
4.73333	0.00001	0.00045	-0.00189	-0.01105	0.00068	AB
4.84061	0.00000	0.00024	-0.00118	-0.00806	0.00045	AB
5.35960	0.00000	0.00000	-0.00004	-0.00118	0.00004	AB
5.94727	0.00000	0.00003	-0.00003	-0.00290	0.00012	AA
5.94727	0.00000	0.00000	0.00000	0.00000	0.00000	BB

Table 6.1: SnS: tight-binding parameters for single zeta basis.

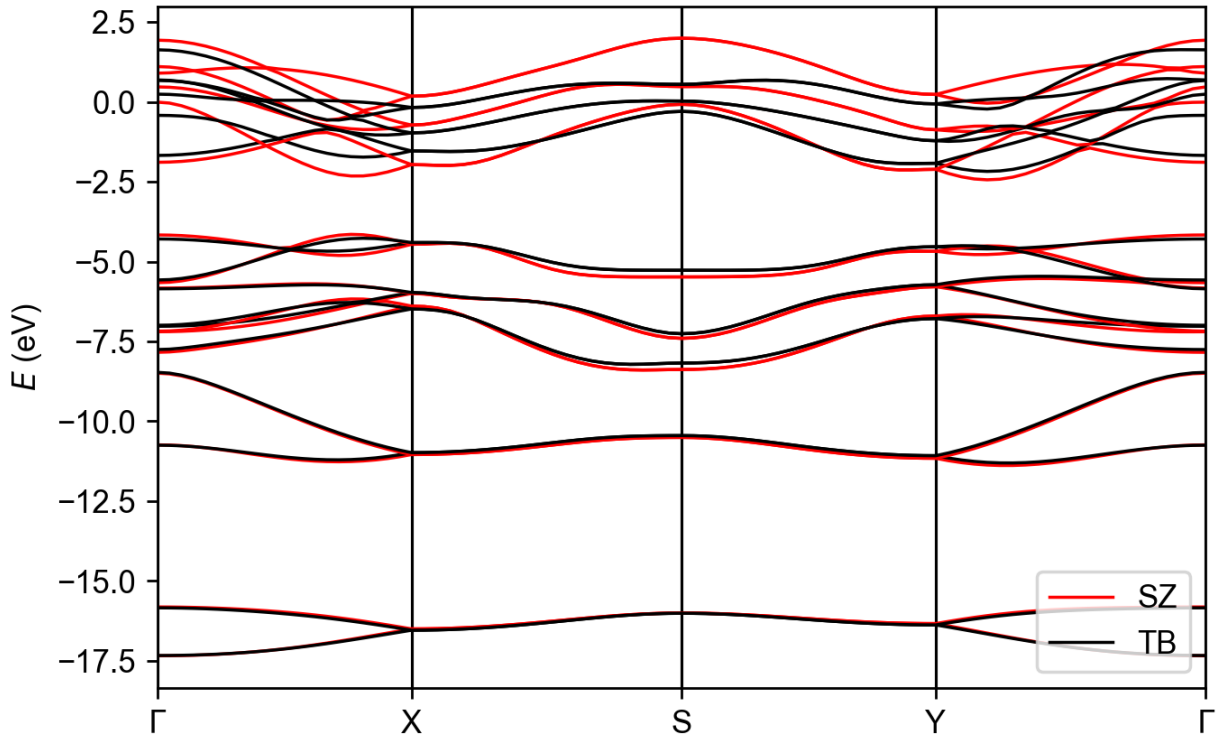


Figure 6.2: SnS electronic band structure. This plots the single zeta (SZ) basis compared with its tight-binding (TB) representation found in Table 6.1.

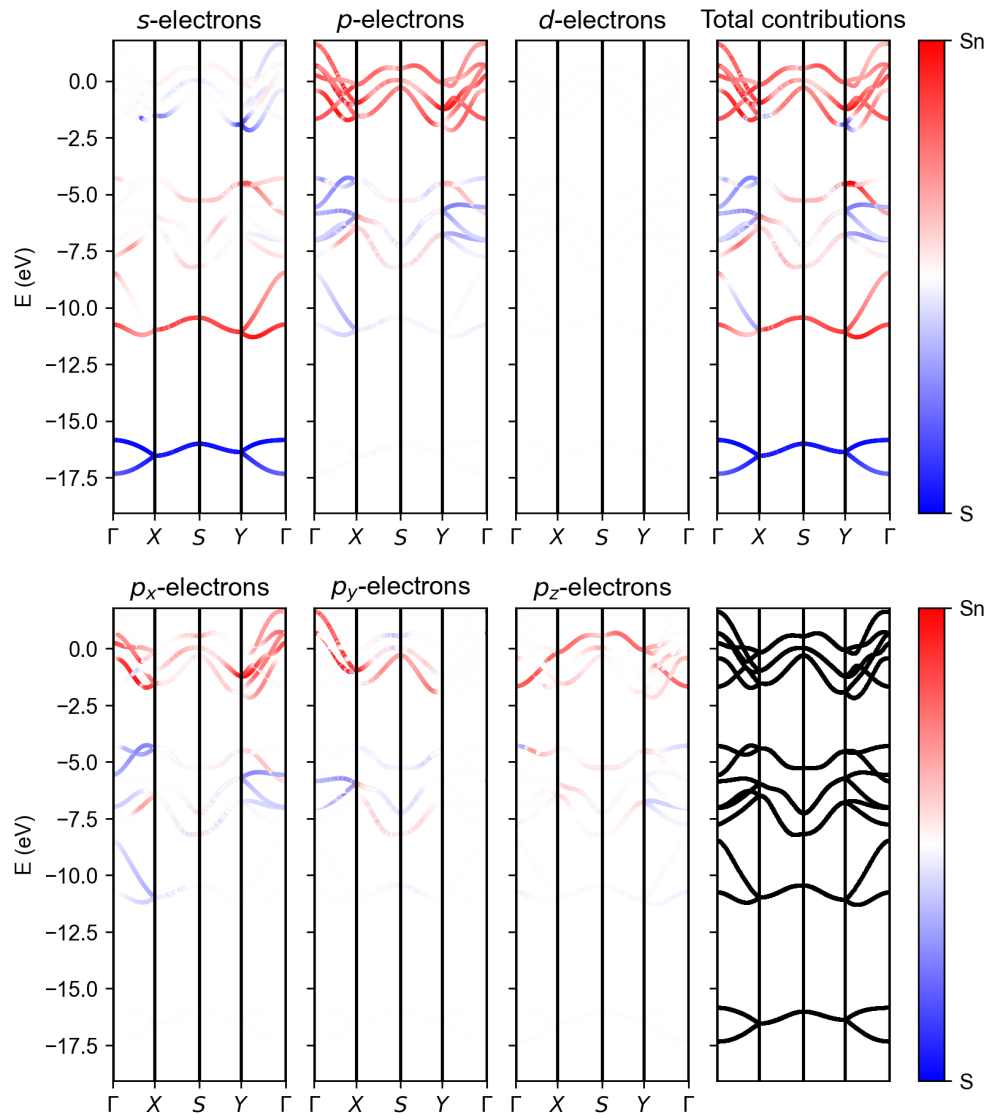


Figure 6.3: Decomposed tight-binding electronic band structure for a SnS monolayer with a numerical atomic orbital basis of *s* and *p* orbitals.

6.1.2 SnS: single zeta polarized basis

This section reports our onsite Hamiltonian matrix, our tight-binding parameters, and our resultant electronic band structure for a single zeta polarized basis. This basis sets an s , p_y , p_z , p_x , d_{xy} , d_{yz} , $d_{z^2-r^2}$, d_{xz} , and $d_{x^2-y^2}$ orbital (in this order) on each atom within our unit cell. Our onsite Hamiltonians are given on the following two pages (the matrices are large).

(6.12)

$$H_{Sn1-Sn1} = \begin{pmatrix} -10.24951 & 0.00000 & 0.85382 & 0.42662 & 0.00000 & 0.00000 & -0.06989 & 0.06263 & 0.09652 \\ 0.00000 & -4.93097 & 0.00000 & 0.00000 & 1.41959 & 0.96808 & 0.00000 & 0.00000 & 0.00000 \\ 0.85382 & 0.00000 & -4.72641 & 0.07711 & 0.00000 & 0.00000 & 1.99693 & -0.15280 & 0.02286 \\ 0.42662 & 0.00000 & 0.07711 & -4.72181 & 0.00000 & 0.00000 & -0.83351 & 1.01380 & -0.12871 \\ 0.00000 & 1.41959 & 0.00000 & 0.00000 & 1.80531 & -0.27102 & 0.00000 & 0.00000 & 0.00000 \\ 0.00000 & 0.96808 & 0.00000 & 0.00000 & -0.27102 & 4.78900 & 0.00000 & 0.00000 & 0.00000 \\ -0.06989 & 0.00000 & 1.99693 & -0.83351 & 0.00000 & 0.00000 & 2.16518 & 0.56736 & -0.19304 \\ 0.06263 & 0.00000 & -0.15280 & 1.01380 & 0.00000 & 0.00000 & 0.56736 & 4.78174 & 0.10947 \\ 0.09652 & 0.00000 & 0.02286 & -0.12871 & 0.00000 & 0.00000 & -0.19304 & 0.10947 & 4.62392 \end{pmatrix}$$

37

$$H_{Sn2-Sn2} = \begin{pmatrix} -10.24951 & 0.00000 & -0.85382 & 0.42662 & 0.00000 & 0.00000 & -0.06990 & -0.06263 & 0.09652 \\ 0.00000 & -4.93097 & 0.00000 & 0.00000 & 1.41959 & -0.96808 & 0.00000 & 0.00000 & 0.00000 \\ -0.85382 & 0.00000 & -4.72641 & -0.07711 & 0.00000 & 0.00000 & -1.99693 & -0.15281 & -0.02286 \\ 0.42662 & 0.00000 & -0.07711 & -4.72181 & 0.00000 & 0.00000 & -0.83351 & -1.01380 & -0.12871 \\ 0.00000 & 1.41959 & 0.00000 & 0.00000 & 1.80531 & 0.27102 & 0.00000 & 0.00000 & 0.00000 \\ 0.00000 & -0.96808 & 0.00000 & 0.00000 & 0.27102 & 4.78899 & 0.00000 & 0.00000 & 0.00000 \\ -0.06990 & 0.00000 & -1.99693 & -0.83351 & 0.00000 & 0.00000 & 2.16517 & -0.56736 & -0.19304 \\ -0.06263 & 0.00000 & -0.15281 & -1.01380 & 0.00000 & 0.00000 & -0.56736 & 4.78174 & -0.10947 \\ 0.09652 & 0.00000 & -0.02286 & -0.12871 & 0.00000 & 0.00000 & -0.19304 & -0.10947 & 4.62392 \end{pmatrix}$$

$$\begin{aligned}
H_{S1-S1} &= \begin{pmatrix} -15.51652 & 0.00000 & 0.40143 & -0.28867 & 0.00000 & 0.00000 & -0.03633 & -0.24232 & 0.04684 \\ 0.00000 & -6.09713 & 0.00000 & 0.00000 & -0.73363 & 0.12998 & 0.00000 & 0.00000 & 0.00000 \\ 0.40143 & 0.00000 & -6.07695 & -0.22506 & 0.00000 & 0.00000 & 1.09946 & -0.06303 & 0.02167 \\ -0.28867 & 0.00000 & -0.22506 & -6.01518 & 0.00000 & 0.00000 & 0.42987 & 0.17331 & -0.07395 \\ 0.00000 & -0.73363 & 0.00000 & 0.00000 & 6.43366 & -0.26930 & 0.00000 & 0.00000 & 0.00000 \\ 0.00000 & 0.12998 & 0.00000 & 0.00000 & -0.26930 & 7.35605 & 0.00000 & 0.00000 & 0.00000 \\ -0.03633 & 0.00000 & 1.09946 & 0.42987 & 0.00000 & 0.00000 & 6.55542 & -0.19857 & -0.06125 \\ -0.24232 & 0.00000 & -0.06303 & 0.17331 & 0.00000 & 0.00000 & -0.19857 & 7.38411 & -0.13730 \\ 0.04684 & 0.00000 & 0.02167 & -0.07395 & 0.00000 & 0.00000 & -0.06125 & -0.13730 & 7.41650 \end{pmatrix} \\
H_{S2-S2} &= \begin{pmatrix} -15.51651 & 0.00000 & -0.40143 & -0.28867 & 0.00000 & 0.00000 & -0.03634 & 0.24232 & 0.04684 \\ 0.00000 & -6.09712 & 0.00000 & 0.00000 & -0.73363 & -0.12999 & 0.00000 & 0.00000 & 0.00000 \\ -0.40143 & 0.00000 & -6.07694 & 0.22506 & 0.00000 & 0.00000 & -1.09946 & -0.06303 & -0.02167 \\ -0.28867 & 0.00000 & 0.22506 & -6.01517 & 0.00000 & 0.00000 & 0.42987 & -0.17332 & -0.07395 \\ 0.00000 & -0.73363 & 0.00000 & 0.00000 & 6.43366 & 0.26930 & 0.00000 & 0.00000 & 0.00000 \\ 0.00000 & -0.12999 & 0.00000 & 0.00000 & 0.26930 & 7.35605 & 0.00000 & 0.00000 & 0.00000 \\ -0.03634 & 0.00000 & -1.09946 & 0.42987 & 0.00000 & 0.00000 & 6.55542 & 0.19857 & -0.06124 \\ 0.24232 & 0.00000 & -0.06303 & -0.17332 & 0.00000 & 0.00000 & 0.19857 & 7.38412 & 0.13730 \\ 0.04684 & 0.00000 & -0.02167 & -0.07395 & 0.00000 & 0.00000 & -0.06124 & 0.13730 & 7.41651 \end{pmatrix}
\end{aligned}
\tag{6.13}$$

Distance (\AA)	H_{ss}	H_{sp}	H_{ps}	$H_{pp\sigma}$	$H_{pp\pi}$	Interaction
2.61027	-2.31879	-3.15548	5.43058	3.54753	-1.37009	AB
2.74396	-1.80189	-2.58777	4.65352	3.25580	-1.09866	AB
3.26945	-0.58176	-1.11624	2.26843	2.09461	-0.47587	AB
3.71036	-0.04665	-0.23422	0.23422	0.61995	-0.07064	BB
4.07657	-0.22699	-0.92776	0.92776	1.82409	-0.37502	AA
4.07657	-0.00909	-0.07984	0.07984	0.30118	-0.02986	BB
4.18884	-0.18296	-0.84370	0.84370	1.88296	-0.34397	AA
4.33032	-0.11945	-0.59283	0.59283	1.37325	-0.24999	AA
4.33032	-0.00049	-0.03018	0.03018	0.16007	-0.01390	BB
4.73341	-0.00321	-0.04124	0.10749	0.30321	-0.03050	AB
4.84065	-0.00107	-0.02848	0.08161	0.24353	-0.02049	AB
5.35959	0.00000	-0.00088	0.01145	0.07648	-0.00487	AB
5.94727	-0.00001	-0.00854	0.00854	0.14854	-0.00846	AA
5.94727	0.00010	0.00198	-0.00198	-0.00979	-0.00068	BB

Distance (\AA)	S_{ss}	S_{sp}	S_{ps}	$S_{pp\sigma}$	$S_{pp\pi}$	Interaction
2.61027	0.09134	0.18958	-0.27298	-0.32472	0.10984	AB
2.74396	0.06928	0.15663	-0.23112	-0.30202	0.08921	AB
3.26945	0.01858	0.06043	-0.10429	-0.19123	0.03500	AB
3.71036	0.00037	0.00461	-0.00461	-0.02363	0.00194	BB
4.07657	0.00657	0.04784	-0.04784	-0.15999	0.02303	AA
4.07657	0.00002	0.00088	-0.00088	-0.00772	0.00046	BB
4.18884	0.00457	0.03794	-0.03794	-0.13766	0.01843	AA
4.33032	0.00278	0.02780	-0.02780	-0.11230	0.01375	AA
4.33032	0.00000	0.00018	-0.00018	-0.00300	0.00014	BB
4.73341	0.00001	0.00045	-0.00189	-0.01105	0.00068	AB
4.84065	0.00000	0.00024	-0.00118	-0.00805	0.00045	AB
5.35959	0.00000	0.00000	-0.00004	-0.00118	0.00004	AB
5.94727	0.00000	0.00003	-0.00003	-0.00290	0.00012	AA
5.94727	0.00000	0.00000	0.00000	0.00000	0.00000	BB

Table 6.2: SnS: (s, p) tight-binding parameters for single zeta polarized basis.

Distance (\AA)	H_{sd}	H_{ds}	$H_{pd\sigma}$	$H_{pd\pi}$	$H_{dp\sigma}$	$H_{d\pi\pi}$	$H_{dd\sigma}$	$H_{dd\pi}$	$H_{dd\delta}$	Interaction
2.61027	-2.16659	-5.77361	0.99557	-1.08623	-1.64575	2.13475	1.06578	0.01369	-0.33128	AB
2.74396	-1.82407	-5.23789	0.94268	-0.90579	-1.92787	1.80312	0.91326	0.16701	-0.32969	AB
3.26945	-0.99571	-2.95510	0.60994	-0.48059	-1.82907	0.96941	0.52945	0.51033	-0.21711	AB
3.71036	-0.37381	-0.37381	0.78632	-0.19697	-0.78632	0.19697	-0.81885	0.49958	-0.04484	BB
4.07657	-1.16156	-1.16156	1.43592	-0.68472	-1.43592	0.68472	-0.35621	1.04316	-0.20763	AA
4.07657	-0.13955	-0.13955	0.43542	-0.08337	-0.43542	0.08337	-0.58571	0.22549	-0.01605	BB
4.18884	-1.08968	-1.08968	1.63300	-0.69821	-1.63300	0.69821	-0.94492	1.16060	-0.10941	AA
4.33032	-0.78260	-0.78260	1.21880	-0.49406	-1.21880	0.49406	-0.60014	0.87299	-0.13912	AA
4.33032	-0.05678	-0.05678	0.25532	-0.04043	-0.25532	0.04043	-0.39342	0.11634	-0.00821	BB
4.73341	-0.07343	-0.17181	0.35926	-0.07158	-0.42943	0.08225	-0.49009	0.19536	-0.01600	AB
4.84065	-0.05238	-0.14105	0.29199	-0.05644	-0.37369	0.05953	-0.43065	0.15939	-0.01316	AB
5.35959	-0.00182	-0.02188	0.12018	-0.01462	-0.12599	0.01422	-0.19453	0.04002	-0.00246	AB
5.94727	-0.01415	-0.01415	0.23097	-0.02348	-0.23097	0.02348	-0.36113	0.06453	-0.00251	AA
5.94727	0.00756	0.00756	-0.01457	-0.00240	0.01457	0.00240	0.01388	0.00491	0.00181	BB
Distance (\AA)	S_{sd}	S_{ds}	$S_{pd\sigma}$	$S_{pd\pi}$	$S_{dp\sigma}$	$S_{d\pi\pi}$	$S_{dd\sigma}$	$S_{dd\pi}$	$S_{dd\delta}$	Interaction
2.61027	0.19302	0.34326	-0.19521	0.16699	0.29735	-0.23108	0.12703	-0.29616	0.08872	AB
2.74396	0.17070	0.30144	-0.19817	0.14222	0.30149	-0.19449	0.15613	-0.27723	0.06573	AB
3.26945	0.08239	0.15266	-0.16679	0.06729	0.24088	-0.08541	0.19154	-0.15612	0.02407	AB
3.71036	0.00846	0.00846	-0.03824	0.00577	0.03824	-0.00577	0.06180	-0.01756	0.00089	BB
4.07657	0.07026	0.07026	-0.18841	0.05274	0.18840	-0.05274	0.21396	-0.11716	0.01484	AA
4.07657	0.00171	0.00171	-0.01358	0.00147	0.01358	-0.00147	0.02393	-0.00465	0.00024	BB
4.18884	0.05673	0.05673	-0.16716	0.04307	0.16716	-0.04307	0.19298	-0.09653	0.00832	AA
4.33032	0.04244	0.04244	-0.14136	0.03294	0.14136	-0.03294	0.17442	-0.07738	0.00832	AA
4.33032	0.00036	0.00036	-0.00554	0.00046	0.00554	-0.00046	0.01027	-0.00151	0.00006	BB
4.73341	0.00088	0.00327	-0.01779	0.00201	0.01806	-0.00196	0.02911	-0.00582	0.00031	AB
4.84065	0.00047	0.00205	-0.01335	0.00137	0.01332	-0.00132	0.02215	-0.00405	0.00013	AB
5.35959	0.00000	0.00008	-0.00221	0.00013	0.00206	-0.00012	0.00384	-0.00040	0.00001	AB
5.94727	0.00006	0.00006	-0.00483	0.00034	0.00483	-0.00034	0.00805	-0.00100	0.00003	AA
5.94727	0.00000	0.00000	0.00000	0.00000	0.00000	0.00000	0.00000	0.00000	0.00000	BB

Table 6.3: SnS: (s, p, d) tight-binding parameters for single zeta polarized basis.

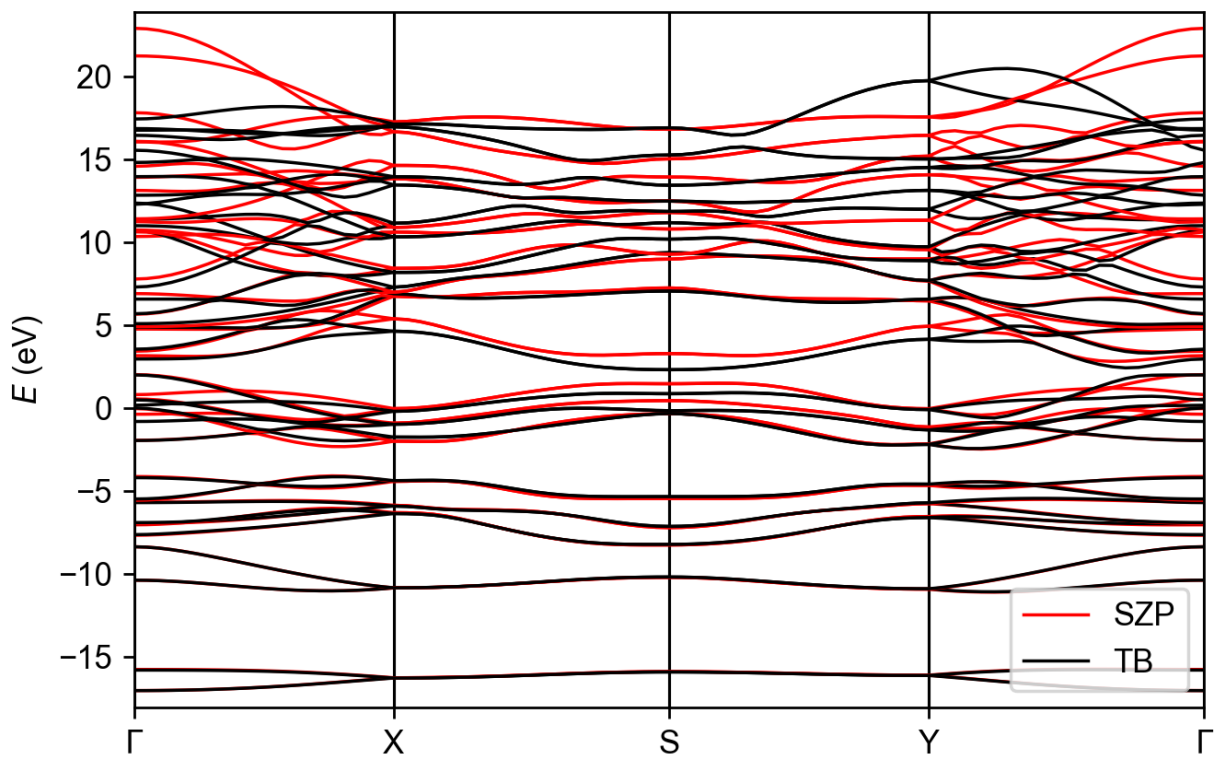


Figure 6.4: SnS electronic band structure. This plots the single zeta polarized (SZP) basis compared with its tight-binding (TB) representation found in Tables 6.2 and 6.3.

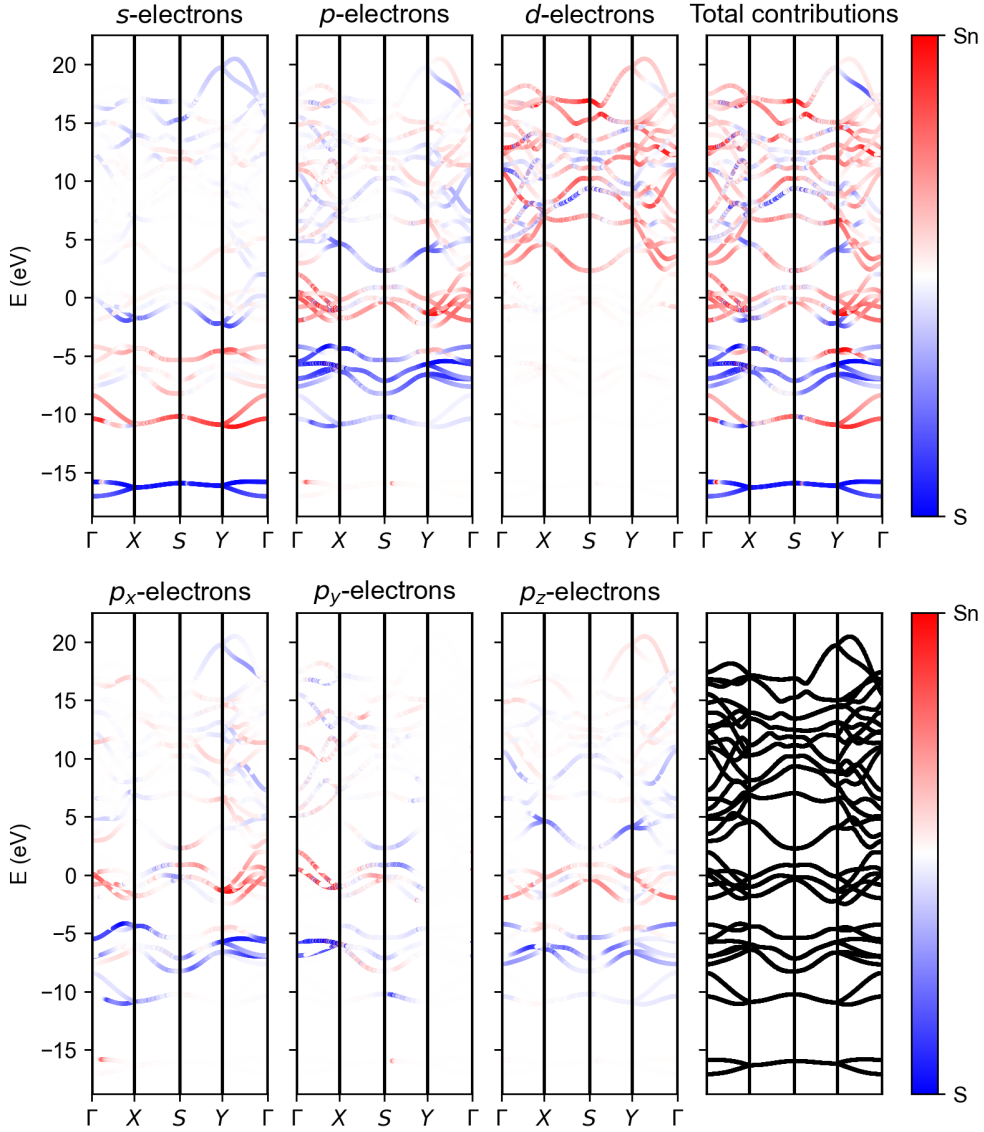


Figure 6.5: Decomposed electronic band structure for a SnS monolayer with a numerical atomic orbital basis of *s*, *p*, and *d* orbitals.

6.1.3 SnTe: single zeta basis

This section reports our onsite Hamiltonian matrix, our tight-binding parameters, and our resultant electronic band structure for a single zeta basis. This basis sets an s , p_y , p_z , and p_x orbital (in this order) on each atom within our unit cell. Our onsite Hamiltonians are given by

$$H_{Sn1-Sn1} = \begin{pmatrix} -10.25684 & 0.00000 & 0.68039 & 0.11006 \\ 0.00000 & -4.78227 & 0.00000 & 0.00000 \\ 0.68039 & 0.00000 & -4.63290 & 0.05212 \\ 0.11006 & 0.00000 & 0.05212 & -4.77500 \end{pmatrix} \quad (6.14)$$

$$H_{Sn2-Sn2} = \begin{pmatrix} -10.25675 & 0.00000 & -0.68043 & 0.11006 \\ 0.00000 & -4.78218 & 0.00000 & 0.00000 \\ -0.68043 & 0.00000 & -4.63283 & -0.05212 \\ 0.11006 & 0.00000 & -0.05212 & -4.77491 \end{pmatrix} \quad (6.15)$$

$$H_{Te1-Te1} = \begin{pmatrix} -13.75305 & 0.00000 & 0.68307 & -0.08050 \\ 0.00000 & -5.48319 & 0.00000 & 0.00000 \\ 0.68307 & 0.00000 & -5.47596 & -0.01700 \\ -0.08050 & 0.00000 & -0.01700 & -5.47735 \end{pmatrix} \quad (6.16)$$

$$H_{Te2-Te2} = \begin{pmatrix} -13.75293 & 0.00000 & -0.68310 & -0.08050 \\ 0.00000 & -5.48308 & 0.00000 & 0.00000 \\ -0.68310 & 0.00000 & -5.47586 & 0.01700 \\ -0.08050 & 0.00000 & 0.01700 & -5.47724 \end{pmatrix} \quad (6.17)$$

Distance (\AA)	H_{ss}	H_{sp}	H_{ps}	$H_{pp\sigma}$	$H_{pp\pi}$	Interaction
2.95535	-1.67746	-2.92898	4.14079	3.53974	-1.10851	AB
3.18220	-1.05907	-2.15541	2.87794	3.05692	-0.87780	AB
3.29371	-0.83995	-1.82132	2.46271	2.77742	-0.74747	AB
4.20905	-0.15950	-0.76209	0.76209	1.67230	-0.30095	AA
4.54994	-0.01141	-0.10823	0.10823	0.43082	-0.04213	BB
4.55900	-0.06014	-0.38990	0.38990	1.08099	-0.16297	AA
4.55900	-0.00990	-0.09850	0.09850	0.38976	-0.03994	BB
4.57000	-0.05827	-0.38132	0.38132	1.06535	-0.15969	AA
4.57000	-0.00926	-0.09524	0.09524	0.38100	-0.03887	BB
5.37558	0.00000	-0.01256	0.03102	0.15831	-0.01132	AB
5.43310	0.00000	-0.00936	0.02757	0.13711	-0.00875	AB
5.50828	0.00000	-0.00601	0.01870	0.11797	-0.00761	AB
6.45519	0.00413	0.01134	-0.01134	0.00608	-0.00327	AA
6.45519	0.00046	0.00294	-0.00294	-0.01335	-0.00232	BB
Distance (\AA)	S_{ss}	S_{sp}	S_{ps}	$S_{pp\sigma}$	$S_{pp\pi}$	Interaction
2.95535	0.06700	0.17932	-0.22044	-0.35105	0.09739	AB
3.18220	0.04070	0.12663	-0.16114	-0.29640	0.06733	AB
3.29371	0.03114	0.10473	-0.13613	-0.26800	0.05550	AB
4.20905	0.00426	0.03634	-0.03634	-0.13384	0.01769	AA
4.54994	0.00004	0.00161	-0.00161	-0.01382	0.00087	BB
4.55900	0.00112	0.01602	-0.01602	-0.07821	0.00832	AA
4.55900	0.00003	0.00155	-0.00155	-0.01346	0.00084	BB
4.57000	0.00107	0.01558	-0.01558	-0.07678	0.00811	AA
4.57000	0.00003	0.00147	-0.00147	-0.01303	0.00081	BB
5.37558	0.00000	0.00006	-0.00028	-0.00423	0.00019	AB
5.43310	0.00000	0.00003	-0.00020	-0.00346	0.00015	AB
5.50828	0.00000	0.00001	-0.00012	-0.00262	0.00010	AB
6.45519	0.00000	0.00000	0.00000	-0.00031	0.00001	AA
6.45519	0.00000	0.00000	0.00000	0.00000	0.00000	BB

Table 6.4: SnTe: tight-binding parameters for single zeta basis.

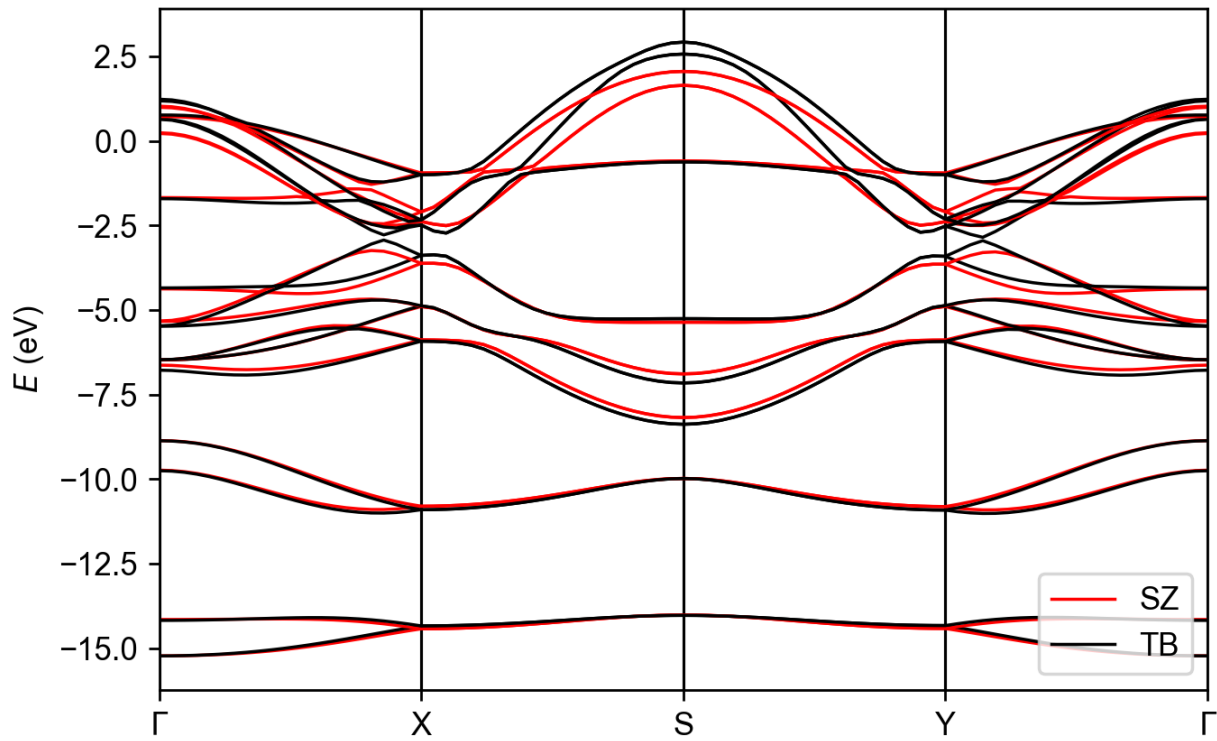


Figure 6.6: SnTe electronic band structure. This plots the single zeta (SZ) basis compared with its tight-binding (TB) representation found in Table 6.4.

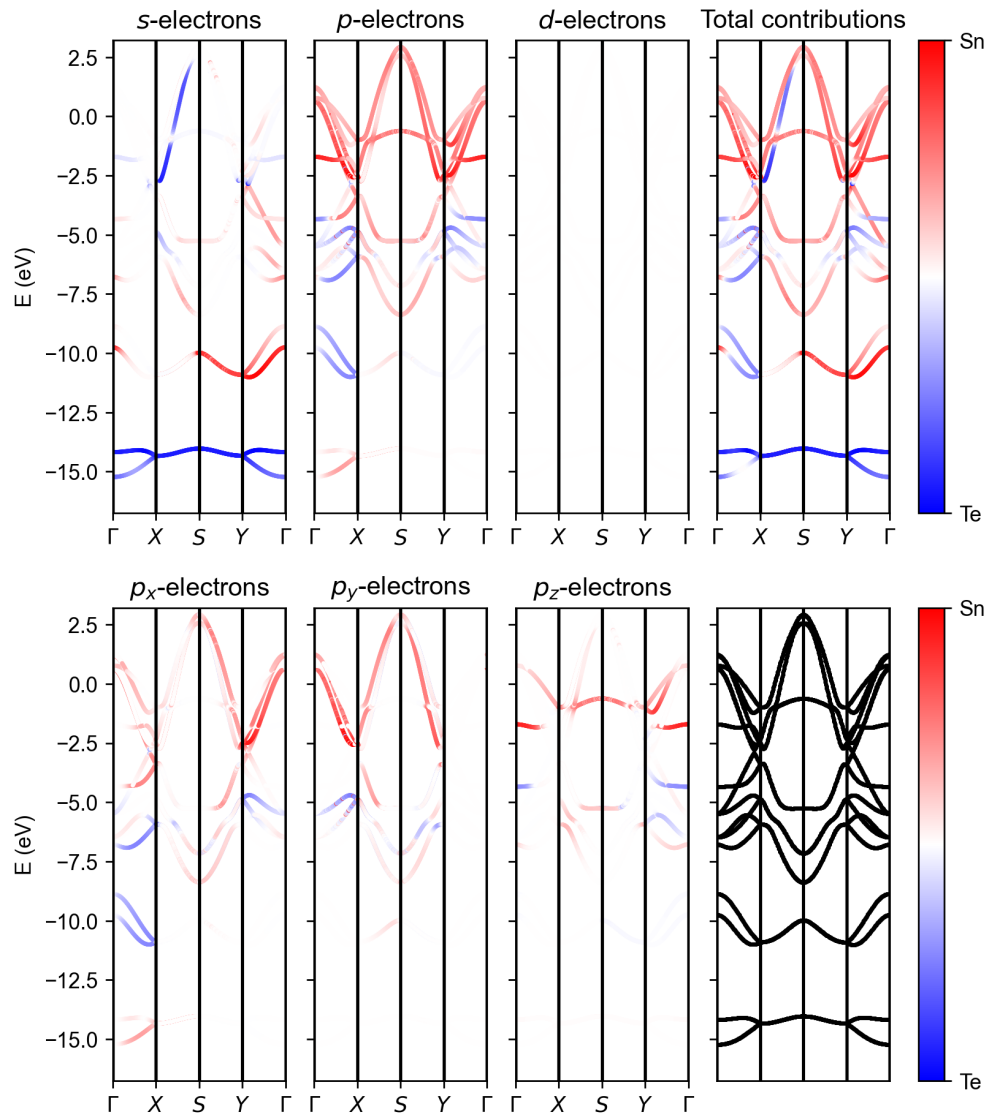


Figure 6.7: Decomposed tight-binding electronic band structure for a SnTe monolayer with a numerical atomic orbital basis of s and p orbitals.

6.1.4 SnTe: single zeta polarized basis

This section reports our onsite Hamiltonian matrix, our tight-binding parameters, and our resultant electronic band structure for a single zeta polarized basis. This basis sets an s , p_y , p_z , p_x , d_{xy} , d_{yz} , $d_{z^2-r^2}$, d_{xz} , and $d_{x^2-y^2}$ orbital (in this order) on each atom within our unit cell. Our onsite Hamiltonians are given on the next two pages by

(6.18)

$$H_{Sn1-Sn1} = \begin{pmatrix} -9.97608 & 0.00000 & 0.46149 & 0.09390 & 0.00000 & 0.00000 & -0.02513 & 0.04077 & 0.00284 \\ 0.00000 & -4.47574 & 0.00000 & 0.00000 & 0.28429 & 0.19835 & 0.00000 & 0.00000 & 0.00000 \\ 0.46149 & 0.00000 & -4.32421 & 0.04896 & 0.00000 & 0.00000 & 1.77618 & 0.00256 & 0.00158 \\ 0.09390 & 0.00000 & 0.04896 & -4.46963 & 0.00000 & 0.00000 & -0.15700 & 0.20152 & -0.00980 \\ 0.00000 & 0.28429 & 0.00000 & 0.00000 & 2.35748 & 0.06348 & 0.00000 & 0.00000 & 0.00000 \\ 0.00000 & 0.19835 & 0.00000 & 0.00000 & 0.06348 & 4.95902 & 0.00000 & 0.00000 & 0.00000 \\ -0.02513 & 0.00000 & 1.77618 & -0.15700 & 0.00000 & 0.00000 & 2.96708 & 0.05817 & -0.00557 \\ 0.04077 & 0.00000 & 0.00256 & 0.20152 & 0.00000 & 0.00000 & 0.05817 & 4.95878 & 0.01153 \\ 0.00284 & 0.00000 & 0.00158 & -0.00980 & 0.00000 & 0.00000 & -0.00557 & 0.01153 & 4.97442 \end{pmatrix}$$

$$H_{Sn2-Sn2} = \begin{pmatrix} -9.97612 & 0.00000 & -0.46148 & 0.09390 & 0.00000 & 0.00000 & -0.02513 & -0.04077 & 0.00284 \\ 0.00000 & -4.47577 & 0.00000 & 0.00000 & 0.28429 & -0.19833 & 0.00000 & 0.00000 & 0.00000 \\ -0.46148 & 0.00000 & -4.32424 & -0.04896 & 0.00000 & 0.00000 & -1.77616 & 0.00256 & -0.00158 \\ 0.09390 & 0.00000 & -0.04896 & -4.46967 & 0.00000 & 0.00000 & -0.15700 & -0.20150 & -0.00980 \\ 0.00000 & 0.28429 & 0.00000 & 0.00000 & 2.35745 & -0.06348 & 0.00000 & 0.00000 & 0.00000 \\ 0.00000 & -0.19833 & 0.00000 & 0.00000 & -0.06348 & 4.95899 & 0.00000 & 0.00000 & 0.00000 \\ -0.02513 & 0.00000 & -1.77616 & -0.15700 & 0.00000 & 0.00000 & 2.96704 & -0.05817 & -0.00557 \\ -0.04077 & 0.00000 & 0.00256 & -0.20150 & 0.00000 & 0.00000 & -0.05817 & 4.95875 & -0.01153 \\ 0.00284 & 0.00000 & -0.00158 & -0.00980 & 0.00000 & 0.00000 & -0.00557 & -0.01153 & 4.97439 \end{pmatrix}$$

(6.19)

$$\begin{aligned}
H_{Te1-Te1} = & \begin{pmatrix} -13.64869 & 0.00000 & 0.38247 & -0.05393 & 0.00000 & 0.00000 & -0.02652 & -0.01335 & 0.00245 \\ 0.00000 & -5.30587 & 0.00000 & 0.00000 & -0.16535 & 0.37514 & 0.00000 & 0.00000 & 0.00000 \\ 0.38247 & 0.00000 & -5.28111 & -0.01416 & 0.00000 & 0.00000 & 0.90651 & -0.00812 & 0.00017 \\ -0.05393 & 0.00000 & -0.01416 & -5.30082 & 0.00000 & 0.00000 & 0.09214 & 0.37548 & -0.00237 \\ 0.00000 & -0.16535 & 0.00000 & 0.00000 & 5.94780 & 0.00898 & 0.00000 & 0.00000 & 0.00000 \\ 0.00000 & 0.37514 & 0.00000 & 0.00000 & 0.00898 & 7.09739 & 0.00000 & 0.00000 & 0.00000 \\ -0.02652 & 0.00000 & 0.90651 & 0.09214 & 0.00000 & 0.00000 & 6.13310 & -0.04285 & -0.00359 \\ -0.01335 & 0.00000 & -0.00812 & 0.37548 & 0.00000 & 0.00000 & -0.04285 & 7.09908 & -0.01297 \\ 0.00245 & 0.00000 & 0.00017 & -0.00237 & 0.00000 & 0.00000 & -0.00359 & -0.01297 & 7.10362 \end{pmatrix} \\
H_{Te2-Te2} = & \begin{pmatrix} -13.64872 & 0.00000 & -0.38246 & -0.05393 & 0.00000 & 0.00000 & -0.02652 & 0.01335 & 0.00245 \\ 0.00000 & -5.30591 & 0.00000 & 0.00000 & -0.16535 & -0.37513 & 0.00000 & 0.00000 & 0.00000 \\ -0.38246 & 0.00000 & -5.28115 & 0.01416 & 0.00000 & 0.00000 & -0.90649 & -0.00812 & -0.00017 \\ -0.05393 & 0.00000 & 0.01416 & -5.30086 & 0.00000 & 0.00000 & 0.09215 & -0.37547 & -0.00237 \\ 0.00000 & -0.16535 & 0.00000 & 0.00000 & 5.94776 & -0.00897 & 0.00000 & 0.00000 & 0.00000 \\ 0.00000 & -0.37513 & 0.00000 & 0.00000 & -0.00897 & 7.09735 & 0.00000 & 0.00000 & 0.00000 \\ -0.02652 & 0.00000 & -0.90649 & 0.09215 & 0.00000 & 0.00000 & 6.13307 & 0.04285 & -0.00359 \\ 0.01335 & 0.00000 & -0.00812 & -0.37547 & 0.00000 & 0.00000 & 0.04285 & 7.09904 & 0.01297 \\ 0.00245 & 0.00000 & -0.00017 & -0.00237 & 0.00000 & 0.00000 & -0.00359 & 0.01297 & 7.10358 \end{pmatrix}
\end{aligned}$$

Distance (\AA)	H_{ss}	H_{sp}	H_{ps}	$H_{pp\sigma}$	$H_{pp\pi}$	Interaction
2.95535	-1.63229	-2.81979	3.99830	3.31636	-1.10440	AB
3.18220	-1.04736	-2.07328	2.89273	2.93071	-0.83738	AB
3.29371	-0.83247	-1.75787	2.48098	2.67548	-0.71412	AB
4.20905	-0.15652	-0.73916	0.73916	1.59066	-0.29099	AA
4.54994	-0.01140	-0.10722	0.10722	0.42145	-0.04188	BB
4.55900	-0.05981	-0.38433	0.38433	1.05612	-0.16062	AA
4.55900	-0.00989	-0.09813	0.09813	0.38617	-0.03994	BB
4.57000	-0.05795	-0.37594	0.37594	1.04116	-0.15742	AA
4.57000	-0.00926	-0.09489	0.09489	0.37755	-0.03889	BB
5.37558	0.00000	-0.01254	0.03086	0.15603	-0.01180	AB
5.43310	0.00000	-0.00934	0.02749	0.13499	-0.00858	AB
5.50828	0.00000	-0.00600	0.01864	0.11660	-0.00795	AB
6.45519	0.00461	0.01161	-0.01161	0.00525	-0.00293	AA
6.45519	0.00047	0.00304	-0.00304	-0.01542	-0.00182	BB
Distance (\AA)	S_{ss}	S_{sp}	S_{ps}	$S_{pp\sigma}$	$S_{pp\pi}$	Interaction
2.95535	0.06700	0.17932	-0.22044	-0.35105	0.09739	AB
3.18220	0.04070	0.12663	-0.16114	-0.29640	0.06733	AB
3.29371	0.03114	0.10473	-0.13613	-0.26800	0.05550	AB
4.20905	0.00426	0.03634	-0.03634	-0.13384	0.01769	AA
4.54994	0.00004	0.00161	-0.00161	-0.01382	0.00087	BB
4.55900	0.00112	0.01602	-0.01602	-0.07821	0.00832	AA
4.55900	0.00003	0.00155	-0.00155	-0.01346	0.00084	BB
4.57000	0.00107	0.01558	-0.01558	-0.07678	0.00811	AA
4.57000	0.00003	0.00147	-0.00147	-0.01303	0.00081	BB
5.37558	0.00000	0.00006	-0.00028	-0.00423	0.00019	AB
5.43310	0.00000	0.00003	-0.00020	-0.00346	0.00015	AB
5.50828	0.00000	0.00001	-0.00012	-0.00262	0.00010	AB
6.45519	0.00000	0.00000	0.00000	-0.00031	0.00001	AA
6.45519	0.00000	0.00000	0.00000	0.00000	0.00000	BB

Table 6.5: SnTe: (s, p) tight-binding parameters for single zeta polarized basis.

Distance (\AA)	H_{sd}	H_{ds}	$H_{pd\sigma}$	$H_{pd\pi}$	$H_{dp\sigma}$	$H_{d\pi}$	$H_{dd\sigma}$	$H_{dd\pi}$	$H_{dd\delta}$	Interaction
2.95535	-2.21651	-4.16198	1.05791	-1.04625	-1.59466	1.65818	1.05725	0.22674	-0.35255	AB
3.18220	-1.79599	-3.19479	1.22632	-0.93461	-1.58649	1.23335	0.73564	0.49759	-0.30155	AB
3.29371	-1.59587	-2.83616	1.15637	-0.83722	-1.57747	1.09031	0.64112	0.56419	-0.26948	AB
4.20905	-0.95873	-0.95873	1.36109	-0.59122	-1.36109	0.59122	-0.64096	0.98444	-0.00799	AA
4.54994	-0.16214	-0.16214	0.53656	-0.10849	-0.53656	0.10849	-0.66132	0.25336	-0.00169	BB
4.55900	-0.53774	-0.53774	1.05570	-0.34653	-1.05570	0.34653	-0.77871	0.68586	-0.08691	AA
4.55900	-0.15164	-0.15164	0.49170	-0.09696	-0.49170	0.09696	-0.58679	0.23026	-0.01989	BB
4.57000	-0.52703	-0.52703	1.04534	-0.34067	-1.04534	0.34067	-0.78017	0.67742	-0.08509	AA
4.57000	-0.14702	-0.14702	0.48246	-0.09456	-0.48246	0.09456	-0.57878	0.22511	-0.01945	BB
5.37558	-0.02159	-0.05081	0.21991	-0.02853	-0.22410	0.03254	-0.32469	0.08517	-0.00306	AB
5.43310	-0.01625	-0.04727	0.19243	-0.02585	-0.20557	0.02681	-0.29794	0.07367	-0.00140	AB
5.50828	-0.01057	-0.03176	0.16858	-0.01981	-0.17484	0.02236	-0.25703	0.05912	-0.00242	AB
6.45519	0.02859	0.02859	0.02135	-0.00625	-0.02135	0.00625	-0.05250	0.01808	-0.00023	AA
6.45519	0.01217	0.01217	-0.02612	-0.00161	0.02612	0.00161	0.04106	0.00440	0.00002	BB
Distance (\AA)	S_{sd}	S_{ds}	$S_{pd\sigma}$	$S_{pd\pi}$	$S_{dp\sigma}$	$S_{d\pi}$	$S_{dd\sigma}$	$S_{dd\pi}$	$S_{dd\delta}$	Interaction
2.95535	0.19840	0.27617	-0.25372	0.16251	0.33102	-0.20167	0.19437	-0.30054	0.07287	AB
3.18220	0.15129	0.21373	-0.24160	0.12018	0.31282	-0.14730	0.22936	-0.24707	0.04833	AB
3.29371	0.12946	0.18518	-0.23034	0.10226	0.29633	-0.12443	0.23365	-0.21753	0.03846	AB
4.20905	0.05450	0.05450	-0.16339	0.04149	0.16339	-0.04149	0.19167	-0.09683	0.00665	AA
4.54994	0.00271	0.00271	-0.02116	0.00240	0.02116	-0.00240	0.03220	-0.00655	0.00027	BB
4.55900	0.02522	0.02522	-0.10376	0.02068	0.10376	-0.02068	0.13625	-0.05077	0.00473	AA
4.55900	0.00261	0.00261	-0.02064	0.00232	0.02064	-0.00232	0.03172	-0.00641	0.00034	BB
4.57000	0.02456	0.02456	-0.10211	0.02021	0.10211	-0.02021	0.13446	-0.04969	0.00459	AA
4.57000	0.00248	0.00248	-0.02003	0.00223	0.02003	-0.00223	0.03083	-0.00617	0.00033	BB
5.37558	0.00010	0.00050	-0.00670	0.00053	0.00707	-0.00056	0.01124	-0.00158	0.00006	AB
5.43310	0.00006	0.00035	-0.00554	0.00042	0.00582	-0.00043	0.00941	-0.00125	0.00003	AB
5.50828	0.00002	0.00021	-0.00425	0.00030	0.00445	-0.00031	0.00722	-0.00088	0.00003	AB
6.45519	0.00000	0.00000	-0.00055	0.00002	0.00055	-0.00002	0.00096	-0.00006	0.00000	AA
6.45519	0.00000	0.00000	0.00000	0.00000	0.00000	0.00000	0.00000	0.00000	0.00000	BB

Table 6.6: SnTe: (s, p, d) tight-binding parameters for single zeta polarized basis.

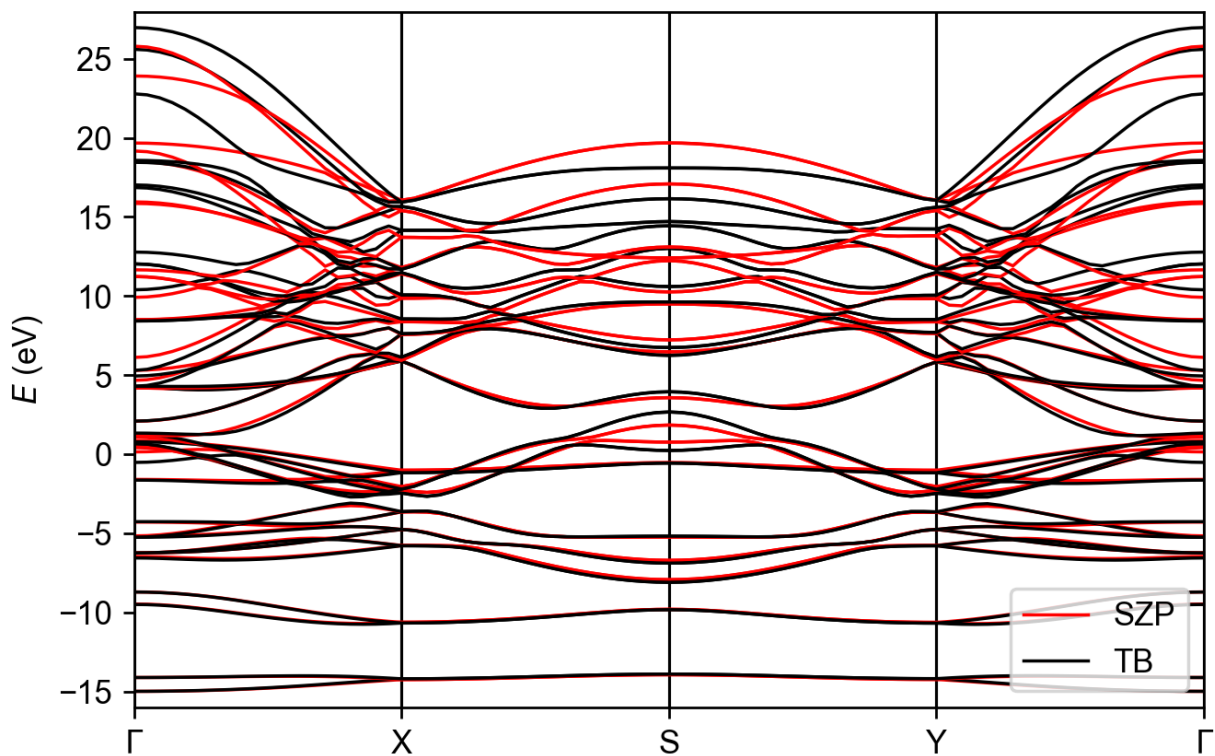


Figure 6.8: SnTe electronic band structure. This plots a single zeta polarized (SZP) basis compared with its tight-binding (TB) representation found in Tables 6.5 and 6.6.

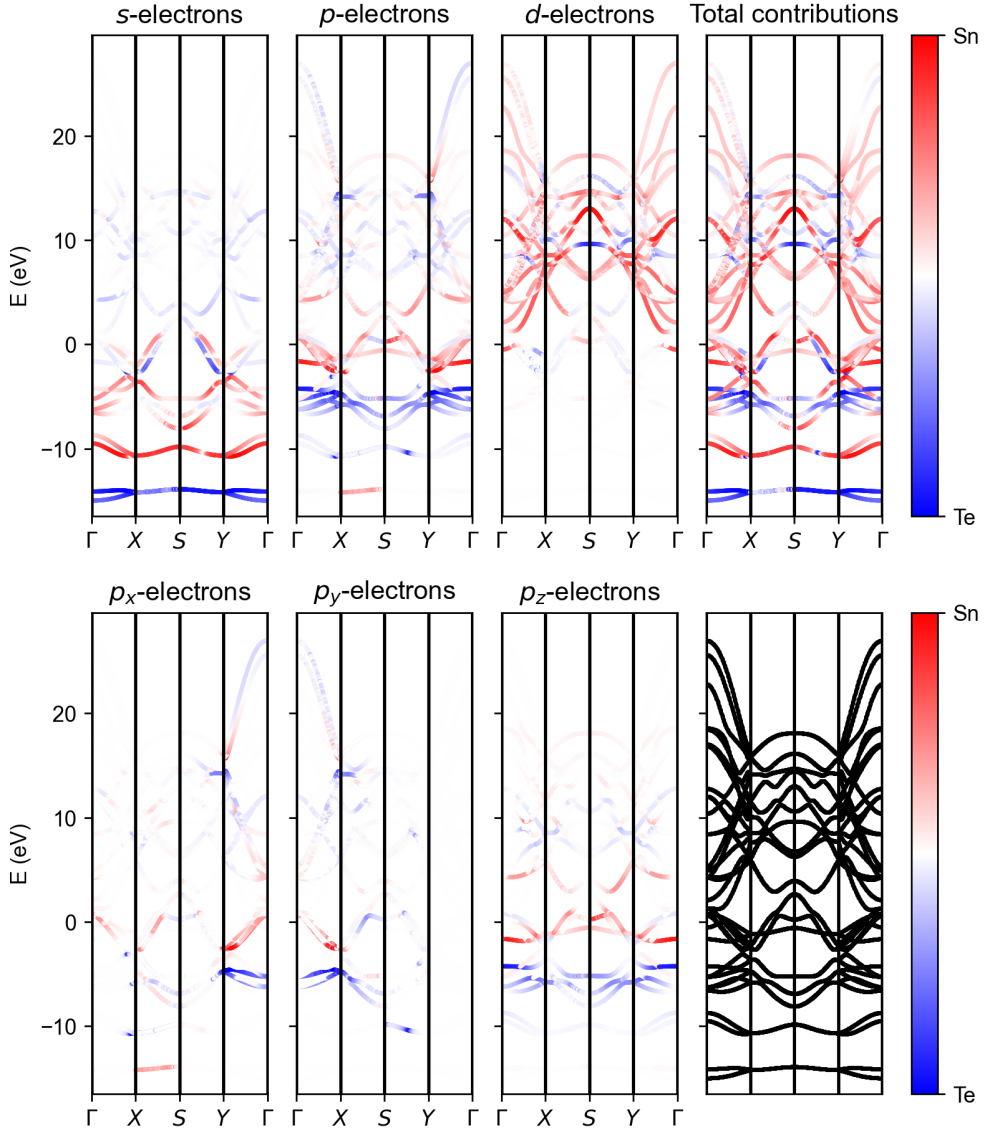


Figure 6.9: Decomposed tight-binding electronic band structure for a SnS monolayer with a numerical atomic orbital basis of *s*, *p*, and *d* orbitals.

Chapter 7

Determining tight-binding parameters

As mentioned previously, I used our standard SIESTA output to determine our tight-binding parameters. This chapter outlines this process.

7.1 Required data files

To keep this process/code generalized, we cannot assume to know (a priori) what atomic species and orbitals we are working with; we first need the `.ORB_INDX` file. The first line contains two values, where we will just use the first; it is the number of orbitals in our unit cell N_u . After two comment lines, we then input the next N_u lines which contain the atomic species and the three quantum numbers (n, l, m) required to identify each orbital. This is then stored for later use. The beginning of this specific data file is shown below.

```
16      480 = orbitals in unit cell and supercell. See end of file.
```

io	ia	is	spec	iao	n	l	m	z	p	sym	rc	isc	iuo
1	1	1	Sn	1	5	0	0	1	F	s	5.275	0	0
2	1	1	Sn	2	5	1	-1	1	F	py	6.773	0	0
3	1	1	Sn	3	5	1	0	1	F	pz	6.773	0	0
4	1	1	Sn	4	5	1	1	1	F	px	6.773	0	0
5	2	1	Sn	1	5	0	0	1	F	s	5.275	0	0
6	2	1	Sn	2	5	1	-1	1	F	py	6.773	0	0
7	2	1	Sn	3	5	1	0	1	F	pz	6.773	0	0
8	2	1	Sn	4	5	1	1	1	F	px	6.773	0	0
9	3	2	S	1	3	0	0	1	F	s	4.168	0	0
10	3	2	S	2	3	1	-1	1	F	py	5.091	0	0
11	3	2	S	3	3	1	0	1	F	pz	5.091	0	0
12	3	2	S	4	3	1	1	1	F	px	5.091	0	0
13	4	2	S	1	3	0	0	1	F	s	4.168	0	0
14	4	2	S	2	3	1	-1	1	F	py	5.091	0	0
15	4	2	S	3	3	1	0	1	F	pz	5.091	0	0
16	4	2	S	4	3	1	1	1	F	px	5.091	0	0
17	5	1	Sn	1	5	0	0	1	F	s	5.275	1	0

I then need the standard input file, `input.fdf`. This is solely to collect information on our lattice vectors, and is declared by the block:

```
%block LatticeVectors
 4.3303193121      0.0000000000      0.0000000000
 0.0000000000      4.0765639097      0.0000000000
 0.0000000000      0.0000000000      29.9986599786
%endblock LatticeVectors
```

We then need the `.HSX` file for the bulk of our data. To get this file, simply set `SaveHS = T` within the `input.fdf` file. This results in a file that contains information on the Hamiltonian (H), Overlap matrix (S), and atomic positions (X_{ij}).

The first line contains information on the number of orbitals within the unit cell N_u , the number of orbitals within the supercell N_s , the number of spins (should be one), and the dimensions of our sparse matrices N_{dim} . This dimension is very useful in the declaration of storage arrays.

The second block contains N_s entries (in lines with 16 entries each) on indices relating orbitals in the supercell to equivalent orbitals in the unit cell.

The third block contains N_u entries (in lines with 4 entries each) and contains the number of non-zero elements per row of the Hamiltonian matrix.

The fourth block contains N_{dim} total entries which help define the sparse data storage for the Hamiltonian and overlap matrices.

The next two blocks (fifth and sixth blocks) contain our sparse Hamiltonian and overlap matrices. Therefore this is not the actual Hamiltonian and overlap matrices used in our eigenvalue problem. The creation of usable matrices just requires a few nested for-loops (which are given explicitly within the SIESTA source code in the `hsx.f90` file). Importantly, the Hamiltonian elements are given in Rydberg and not electron-Volts.

The final block (seventh block) contains the positional data \mathbf{R}_i for all atoms within our supercell. Importantly, these position vectors are given in Bohr and not Angstroms. This data is then used in determining the phase ($e^{i\mathbf{k} \cdot \mathbf{R}_i}$) of given matrix entries and for determining the distance of any given orbital interaction.

7.2 Systems of equations

Once all of this data is stored, we can then determine our tight-binding parameters. To do so, we first need to determine the normalized position vectors (projection cosines) for all \mathbf{R}_i . At this stage, we also determine our unique distances for interactions (Distance (Å) column within prior Tables).

We then cycle over all possible interactions within the sparse matrices, saving which specific interactions connect $s - s$ orbitals. Let any sparse element in question be denoted by T . Looking at Table B.1, we see that our tight-binding parameter must simply be $V_{ss} = T$. So when we determine our $s - s$ interactions, we simply find the average of all sparse elements per distance/interaction. This is our V_{ss} value.

We then cycle over all possible interactions within the sparse matrices, saving which specific interactions connect $s - p$ orbitals. Let any sparse element in question be denoted by T . Once we determine which are $s - p$ interactions, we have three possibilities: $s - p_x$, $s - p_y$, and $s - p_z$. Looking at Table B.1, we see that our tight-binding parameter must satisfy

$$\begin{aligned} s - p_x &\implies \ell V_{sp} = T \implies V_{sp} = T/\ell \\ s - p_y &\implies m V_{sp} = T \implies V_{sp} = T/m \\ s - p_z &\implies n V_{sp} = T \implies V_{sp} = T/n \end{aligned} \quad (7.1)$$

respectively and assuming the correlated projection cosine is non-zero. We then find the average of these V_{sp} for a given distance/interaction, where that is reported.

We then cycle over all possible interactions within the sparse matrices, saving which specific interactions connect $p - s$ orbitals. Let any sparse element in question be denoted by T . Once we determine which are $p - s$ interactions, we have three possibilities: $p_x - s$, $p_y - s$, and $p_z - s$. Looking at Table B.1, we see that our tight-binding parameter must satisfy

$$\begin{aligned} p_x - s &\implies \ell V_{ps} = T \implies V_{ps} = T/\ell \\ p_y - s &\implies m V_{ps} = T \implies V_{ps} = T/m \\ p_z - s &\implies n V_{ps} = T \implies V_{ps} = T/n \end{aligned} \quad (7.2)$$

respectively and assuming the correlated projection cosine is non-zero. We then find the average of these V_{ps} for a given distance/interaction, where that is reported.

We then cycle over all possible interactions within the sparse matrices, saving which specific interactions connect $p - p$ orbitals. Let any sparse element in question be denoted by T . Once we determine which are $p - p$ interactions, we have nine possibilities:

$$\begin{aligned} p_x - p_x &\implies \ell^2 V_{pp}^\sigma + (1 - \ell^2) V_{pp}^\pi = T \\ p_y - p_y &\implies m^2 V_{pp}^\sigma + (1 - m^2) V_{pp}^\pi = T \\ p_z - p_z &\implies n^2 V_{pp}^\sigma + (1 - n^2) V_{pp}^\pi = T \\ p_x - p_y &\implies \ell m V_{pp}^\sigma - \ell m V_{pp}^\pi = T \\ p_y - p_x &\implies \ell m V_{pp}^\sigma - \ell m V_{pp}^\pi = T \\ p_x - p_z &\implies \ell n V_{pp}^\sigma - \ell n V_{pp}^\pi = T \\ p_z - p_x &\implies \ell n V_{pp}^\sigma - \ell n V_{pp}^\pi = T \\ p_y - p_z &\implies n m V_{pp}^\sigma - n m V_{pp}^\pi = T \\ p_z - p_y &\implies n m V_{pp}^\sigma - n m V_{pp}^\pi = T. \end{aligned} \quad (7.3)$$

Didactically, assume we have two interactions which are $p_x - p_x$ and $p_x - p_y$. By Table B.1,

and Equation 7.3, we must have

$$\begin{aligned} \ell^2 V_{pp}^\sigma + (1 - \ell^2) V_{pp}^\pi &= T_1 \\ \ell m V_{pp}^\sigma - \ell m V_{pp}^\pi &= T_2 \end{aligned} \implies \begin{pmatrix} \ell^2 & 1 - \ell^2 \\ \ell m & -\ell m \end{pmatrix} \begin{pmatrix} V_{pp}^\sigma \\ V_{pp}^\pi \end{pmatrix} = \begin{pmatrix} T_1 \\ T_2 \end{pmatrix} \quad (7.4)$$

$$\implies \begin{pmatrix} V_{pp}^\sigma \\ V_{pp}^\pi \end{pmatrix} = \begin{pmatrix} \ell^2 & 1 - \ell^2 \\ \ell m & -\ell m \end{pmatrix}^{-1} \begin{pmatrix} T_1 \\ T_2 \end{pmatrix}. \quad (7.5)$$

This then gives us values for our two tight-binding parameters assuming this matrix is invertible. To check if this inverse exists, simply see if its determinant is non-zero. So we now have one value for V_{pp}^σ and one value for V_{pp}^π . To find an average for any given distance/interaction, we perform this system of equations for all possible interactions. Therefore if one distance/interaction has three sparse elements $\{A, B, C\}$, we solve our system of equations for $\{A, B\}$, $\{A, C\}$, and $\{B, C\}$ then find its averages. The fact that interactions of two p orbitals are facilitated by *two* parameters is why we need this system of equations.

We then cycle over all possible interactions within the sparse matrices, saving which specific interactions connect $s - d$ orbitals. Let any sparse element in question be denoted by T . Once we determine which are $s - d$ interactions, we have five possibilities: $s - d_{xy}$, $s - d_{yz}$, $s - d_{zx}$, $s - d_{x^2-y^2}$, and $s - d_{3z^2-r^2}$. By Table B.1 we must have

$$\begin{aligned} s - d_{xy} &\implies \sqrt{3}\ell m V_{sd} = T &&\implies V_{sd} = T/\sqrt{3}\ell m \\ s - d_{yz} &\implies \sqrt{3}mn V_{sd} = T &&\implies V_{sd} = T/\sqrt{3}mn \\ s - d_{zx} &\implies \sqrt{3}\ell n V_{sd} = T &&\implies V_{sd} = T/\sqrt{3}\ell n \\ s - d_{x^2-y^2} &\implies \frac{1}{2}\sqrt{3}(\ell^2 - m^2)V_{sd} = T &&\implies V_{sd} = 2T/[\sqrt{3}(\ell^2 - m^2)] \\ s - d_{3z^2-r^2} &\implies \left[n^2 - \frac{1}{2}(\ell^2 + m^2)\right]V_{sd} = T &&\implies V_{sd} = T/\left[n^2 - \frac{1}{2}(\ell^2 + m^2)\right]. \end{aligned} \quad (7.6)$$

This obviously assumes we do not divide by zero. We then find the average of these V_{sd} for a given distance/interaction, where that is reported.

This general process is then repeated for $d - s$ interactions. For $p - d$ and $d - p$ interactions, we have a linear system of two equations as with the $p - p$ interactions. Then for $d - d$ interactions, we have a linear system of three equations which is solved in the same way as before but using Table B.2.

This then has determined all possible tight-binding parameters for an arbitrary system. Note that we assume that all p orbitals can be treated equally and that all d orbitals can be treated equally. This still produces accurate results while significantly reducing the total number of parameters. This is important if anyone wants to optimize these parameters to fit a given electronic band structure. We actually did this successfully for our SnS monolayer using the Nelder-Mead (Simplex) optimization algorithm [42], but we wanted to take this project in a different direction.

Chapter 8

Future developments

At this stage in the project, we are able to automatically obtain a tight-binding representation upon completion of a self-consistent SIESTA calculation. As such, the next logical step is to append my subroutines to our local SIESTA compilation which has been completed. The application of this is to numerically determine light-matter interactions, namely second-harmonic generation (SHG) as hinted within the Motivation (Chapter 1). Here at the University of Arkansas, that is the focus of Dr. Debajit Chakraborty and Luis Enrique Rosas Hernandez's work; the calculation of the second-order optical susceptibility tensor. They have successfully implemented these subroutines for the simulation of SHG through Fourier transformations, and are currently coding the more accurate $\mathbf{k} \cdot \mathbf{p}$ approximation.

The main difficulty present is the cost of computations, which increases rapidly as our expressions include several nested integrals. There have been creative solutions, though, including implementing external results through SIESTA subroutines and parallelization on our local clusters. Data is currently being obtained and verified for these systems on group-IV monochalcogenides and transition-metal dichalcogenide monolayers.

Ideally, all these scripts could be added to SIESTA, natively supporting tight-binding parameters for general output and the calculation of the second-order susceptibility tensor. Once these are functioning, one could even determine the effects of defects on light-matter interactions as they will break many symmetries. There is rich physics available within these systems, and our developments are making strides to better understand two-dimensional ferroelectrics.

Appendix A

Algorithm to check inversion symmetry

```
PROGRAM MAIN
```

```
IMPLICIT NONE
```

```
INTEGER ii ,ii2 , jj , kk , ll , t ,numInv ,numPts ,numAtoms(10)
```

```
INTEGER totAtoms ,numElems ,origInd ,sup_cell ,numSpecies
```

```
REAL Amat(3 ,3) ,AmatInv(3 ,3) ,new_vec(3) ,conv_crit
```

```
CHARACTER selDynamCheck(1) ,mat_type(1)
```

```
CHARACTER(LEN=3) file_status
```

```
LOGICAL inv_symm ,file_exists
```

```
REAL,ALLOCATABLE :: vec (:,:,:), vec_super (:,:,:)
```

```
REAL,ALLOCATABLE :: inv_points (:,:)
```

```
REAL,ALLOCATABLE :: pts2chk (:,:)
```

```
!-----!
```

```
conv_crit = 1e-2 !convergence criterion for inversion point
```

```
numSpecies = 2 !number of atomic species within the material
```

```
!-----!
```

```
inv_symm = .false.
```

```
open(unit=1,file='POSCAR',status='old') !opens file for input
```

```
Amat = 0.0
```

```
read(1,*)
```

```
read(1,*)
```

```

read(1,* ) Amat(:,1) ! reads a1
read(1,* ) Amat(:,2) ! reads a2
read(1,* ) Amat(:,3) ! reads a3
read(1,* )

! finds inverse of (a1,a2,a3) matrix
call M33INV(Amat,AmatInv)

numAtoms = 0
read(1,* ) numAtoms(1:numSpecies)

totAtoms = sum(numAtoms) ! total atoms per unit cell
numElems = 10 - count(numAtoms==0) !# of species per u.c.
allocate(vec(numElems,maxval(numAtoms),3)) !pos of atoms in u.c.

read(1,* ) selDynamCheck ! if POSCAR has 'Selective dynamics' tag
if (selDynamCheck(1) == 's' .or. selDynamCheck(1) == 'S') then
    read(1,* ) selDynamCheck
endif

vec = 0 ! reads atomic positions
do ii=1,numElems
    do jj=1,numAtoms(ii)
        read(1,* ) vec(ii,jj,:)
    enddo !jj
enddo !ii
!vec( atomic species , index per atomic species , (x,y,z) )
close(1)

! This converts from cartesian to direct coords (if needed)
if (selDynamCheck(1) == 'c' .or. selDynamCheck(1) == 'C') then
    do ii=1,numElems
        do jj=1,numAtoms(ii)
            vec(ii,jj,:) = matmul(AmatInv,vec(ii,jj,:))
        enddo !jj
    enddo !ii
endif

write(*,'(a37)',advance='no') 'Is this material slab or bulk? (s/b)'
read(*,* ) mat_type ! stores whether material is slab or bulk

! finds supercell to check for inversion point
if (mat_type(1) == 's' .or. mat_type(1) == 'S') then ! slab
    sup_cell = 0 ! checks a1,a2 in (-1,0,1)
else if (mat_type(1) == 'b' .or. mat_type(1) == 'B') then ! bulk

```

```

    sup_cell = 1 ! checks a1,a2,a3 in (-1,0,1)
else ! error check
    write(*,*) 'Error: _first_character_must_be_"s/S_or_b/B"'
    call exit(0)
endif

origInd = minloc(numAtoms(1:numElems),1) ! index for least # of elem
allocate(pts2chk(numAtoms(origInd)*9*(1+2*sup_cell),3))
allocate(inv_points(numAtoms(origInd)*9*(1+2*sup_cell),3))
allocate(vec_super(numElems,maxval(numAtoms)*9*(1+2*sup_cell),3))

numPts = 0 ! indexes inversion point (in u.c.) we are analyzing
do ii=1,numAtoms(origInd)
do jj=-1,1
    do kk=-1,1
        do ll=-sup_cell,sup_cell
            new_vec(:) = (vec(origInd,1,:)+vec(origInd,ii,:)) &
                + (/jj,kk,ll/))/2
            ! checks if inversion point is in unit cell
            if (0 <= minval(new_vec).and. maxval(new_vec) <= 1) then
                numPts = numPts + 1
                ! Finds inversion points to check, which are the
                ! midway points on lines connecting given origin
                ! atom [ vec(origInd,1,:) ] and other atoms in
                ! the supercell of the same species.
                pts2chk(numPts,:)=new_vec(:)
            endif
        enddo
    enddo !kk
enddo !jj
enddo !ii

! Makes supercell, for more straight-forward inversion point checking
vec_super = 0 ! reads atomic positions
do ii=1,numElems
    t = 0 ! indexes number of atoms per given atomic species
    do ii2=1,numAtoms(ii)
        do jj=-1,1
            do kk=-1,1
                do ll=-sup_cell,sup_cell
                    t = t + 1
                    vec_super(ii,t,:)=vec(ii,ii2,:)+(/jj,kk,ll/)
                enddo !ll
            enddo !kk
        enddo !jj
    enddo

```

```

enddo ! i i2
enddo ! i i

! Checks each inversion point with each element within u.c.
numInv = 0 ! indexes number of confirmed inversion points
do ii=1,numPts
    t = 0 ! indexes which inversion point we are analyzing

    do jj=1,numElems
        do kk=1,numAtoms(jj)
            ! inverts atomic pos from u.c. through point of interest
            new_vec(:) = 2*pts2chk(ii,:)-vec(jj,kk,:)

            ! checks for new_vec within our supercell
            do ll=1,numAtoms(jj)*9*(1+2*sup_cell)
                if (norm2(new_vec(:)-vec_super(jj,ll,:))<conv_crit)then
                    ! adds one when point works with given inv point
                    t = t + 1
                endif
            enddo ! ll

            enddo ! kk
    enddo ! jj

! runs when every point in unit cell works with inversion point
if (t == sum(numAtoms)) then
    inv_symm = .true.
    numInv = numInv + 1
    inv_points(numInv,:) = pts2chk(ii,:)
endif

! runs if too many points work for inversion point
if (t > sum(numAtoms)) then
    write(*,*) 'Error: Convergence criteria is too large'
    call exit(0)
endif

enddo ! ii

if (inv_symm .eqv. .true.) then
    write(*,'(a32)') 'Material is inversion symmetric!'
    write(*,'(a26)') 'Inversion points (direct):'
    do ii=1,numInv
        write(*,'(3f10.5)') inv_points(ii,:)
    enddo ! ii

```

```

!Opens output file (if inversion symmetric)
inquire(file='inv_trans.dat',exist=file_exists) !checks for file
if (file_exists .eqv. .true.) then
    file_status(:) = 'old' !if file exists, override it
else
    file_status(:) = 'new' !if file doesn't exist, make it
endif
open(unit=11,file='inv_trans.dat',status=file_status)

write(11,'(a28)') '! (inversion_point_in_direct)'
write(11,'(a41)',advance='no') '! (starting_atom) -->&
                                         (point_after_invert)'
write(11,'(a45)') !(point_in_supercell), distance_between_them'
write(11,*)

do i i=1,numInv

    write(11,'(a1,3f10.5,a1)') '( ,inv_points(ii,:), )'

    do jj=1,numElems
        do kk=1,numAtoms(jj)
            !converts atomic pos from u.c. through point of interest
            new_vec(:) = 2*pts2chk(ii,:) - vec(jj,kk,:)

            !checks for new_vec within our supercell
            do ll=1,numAtoms(jj)*9*(1+2*sup_cell)
                if (norm2(new_vec(:)-vec_super(jj,ll,:))<conv_crit)then
                    write(11,'(a1,3f10.5,a7,3f10.5,a2)',advance='no') &
                        '( ,vec(jj,kk,:), )-->( ,new_vec(:), )',
                    write(11,'(a2,3f10.5,a1)',advance='no') &
                        '( ,vec_super(jj,ll,:), )',
                    write(11,'(f10.5)') norm2(new_vec(:)-vec_super(jj,ll,:))
                endif
            enddo !ll

            enddo !kk
            enddo !jj

        write(11,*)
    enddo !ii

close(11) !closes output file

else

```

```

write(* , '(a35) ') 'Material is not inversion-symmetric!'
endif

```

END PROGRAM MAIN

*!this finds inverse of 3x3 matrix. I avoided using LAPACK
!for easier compilations across machines. Modified from
!https://caps.gsfc.nasa.gov/simpson/software/m33inv_f90.txt*

SUBROUTINE M33INV (A, AINV)

IMPLICIT NONE

```

REAL, DIMENSION(3,3), INTENT(IN) :: A
REAL, DIMENSION(3,3), INTENT(OUT) :: AINV

```

```

REAL, PARAMETER :: EPS = 1.0e-10

```

```

REAL :: DET

```

```

REAL, DIMENSION(3,3) :: COFACTOR

```

```

DET = A(1,1)*A(2,2)*A(3,3) &
      - A(1,1)*A(2,3)*A(3,2) &
      - A(1,2)*A(2,1)*A(3,3) &
      + A(1,2)*A(2,3)*A(3,1) &
      + A(1,3)*A(2,1)*A(3,2) &
      - A(1,3)*A(2,2)*A(3,1)

```

```

IF (ABS(DET) .LE. EPS) THEN

```

```

    AINV = 0.0D0

```

```

    RETURN

```

```

END IF

```

```

COFACTOR(1,1) = +(A(2,2)*A(3,3)-A(2,3)*A(3,2))

```

```

COFACTOR(1,2) = -(A(2,1)*A(3,3)-A(2,3)*A(3,1))

```

```

COFACTOR(1,3) = +(A(2,1)*A(3,2)-A(2,2)*A(3,1))

```

```

COFACTOR(2,1) = -(A(1,2)*A(3,3)-A(1,3)*A(3,2))

```

```

COFACTOR(2,2) = +(A(1,1)*A(3,3)-A(1,3)*A(3,1))

```

```

COFACTOR(2,3) = -(A(1,1)*A(3,2)-A(1,2)*A(3,1))

```

```

COFACTOR(3,1) = +(A(1,2)*A(2,3)-A(1,3)*A(2,2))

```

```

COFACTOR(3,2) = -(A(1,1)*A(2,3)-A(1,3)*A(2,1))

```

```

COFACTOR(3,3) = +(A(1,1)*A(2,2)-A(1,2)*A(2,1))

```

```

AINV = TRANSPOSE(COFACTOR) / DET

```

```

RETURN

```

END SUBROUTINE M33INV

Appendix B

Slater-Koster expressions for tight-binding representations

ϕ_1	ϕ_2	Expression
s	s	$(ss\sigma)$
s	p_x	$l(sp\sigma)$
p_x	p_x	$l^2(pp\sigma) + (1 - l^2)(pp\pi)$
p_x	p_y	$lm(pp\sigma) - lm(pp\pi)$
p_x	p_z	$ln(pp\sigma) - ln(pp\pi)$
s	d_{xy}	$\sqrt{3}lm(sd\sigma)$
s	$d_{x^2-y^2}$	$\frac{1}{2}\sqrt{3}(l^2 - m^2)(sd\sigma)$
s	$d_{3z^2-r^2}$	$\left[n^2 - \frac{1}{2}(l^2 + m^2)\right](sd\sigma)$
p_x	d_{xy}	$\sqrt{3}l^2m(pd\sigma) + m(1 - 2l^2)(pd\pi)$
p_x	d_{yz}	$\sqrt{3}lmn(pd\sigma) - 2lmn(pd\pi)$
p_x	d_{zx}	$\sqrt{3}l^2n(pd\sigma) + n(1 - 2l^2)(pd\pi)$
p_x	$d_{x^2-y^2}$	$\frac{1}{2}\sqrt{3}l(l^2 - m^2)(pd\sigma) + l(1 - l^2 + m^2)(pd\pi)$
p_y	$d_{x^2-y^2}$	$\frac{1}{2}\sqrt{3}m(l^2 - m^2)(pd\sigma) - m(1 + l^2 - m^2)(pd\pi)$
p_z	$d_{x^2-y^2}$	$\frac{1}{2}\sqrt{3}n(l^2 - m^2)(pd\sigma) - n(l^2 - m^2)(pd\pi)$
p_x	$d_{3z^2-r^2}$	$l[n^2 - \frac{1}{2}(l^2 + m^2)](pd\sigma) - \sqrt{3}ln^2(pd\pi)$
p_y	$d_{3z^2-r^2}$	$m[n^2 - \frac{1}{2}(l^2 + m^2)](pd\sigma) - \sqrt{3}mn^2(pd\pi)$
p_z	$d_{3z^2-r^2}$	$n[n^2 - \frac{1}{2}(l^2 + m^2)](pd\sigma) + \sqrt{3}n(l^2 + m^2)(pd\pi)$

Table B.1: Interactions from two-centered integrals for $s - s$, $s - p$, $p - p$, $s - d$, and $p - d$ orbitals as discussed by Slater and Koster [41]. This utilizes a normalized position vector $\hat{\mathbf{r}} = (l, m, n)$ between interacting orbitals.

ϕ_1	ϕ_2	Expression
d_{xy}	d_{xy}	$3l^2m^2(dd\sigma) + (l^2 + m^2 - 4l^2m^2)(dd\pi) + (n^2 + l^2m^2)(dd\delta)$
d_{xy}	d_{yz}	$3lm^2n(dd\sigma) + ln(1 - 4m^2)(dd\pi) + ln(m^2 - 1)(dd\delta)$
d_{xy}	d_{zx}	$3l^2mn(dd\sigma) + mn(1 - 4l^2)(dd\pi) + mn(l^2 - 1)(dd\delta)$
d_{xy}	$d_{x^2-y^2}$	$\frac{3}{2}lm(l^2 - m^2)(dd\sigma) + 2lm(m^2 - l^2)(dd\pi) + \frac{1}{2}lm(l^2 - m^2)(dd\delta)$
d_{yz}	$d_{x^2-y^2}$	$\frac{3}{2}mn(l^2 - m^2)(dd\sigma) - mn[1 + 2(l^2 - m^2)](dd\pi) + mn[1 + \frac{1}{2}(l^2 - m^2)](dd\delta)$
d_{zx}	$d_{x^2-y^2}$	$\frac{3}{2}nl(l^2 - m^2)(dd\sigma) + nl[1 - 2(l^2 - m^2)](dd\pi) - nl[1 - \frac{1}{2}(l^2 - m^2)](dd\delta)$
d_{xy}	$d_{3z^2-r^2}$	$\sqrt{3}lm[n^2 - \frac{1}{2}(l^2 + m^2)](dd\sigma) - 2\sqrt{3}lmn^2(dd\pi) + \frac{1}{2}\sqrt{3}lm(1 + n^2)(dd\delta)$
d_{yz}	$d_{3z^2-r^2}$	$\sqrt{3}mn[n^2 - \frac{1}{2}(l^2 + m^2)](dd\sigma) + \sqrt{3}mn(l^2 + m^2 - n^2)(dd\pi) - \frac{1}{2}\sqrt{3}mn(l^2 + m^2)(dd\delta)$
d_{zx}	$d_{3z^2-r^2}$	$\sqrt{3}ln[n^2 - \frac{1}{2}(l^2 + m^2)](dd\sigma) + \sqrt{3}ln(l^2 + m^2 - n^2)(dd\pi) - \frac{1}{2}\sqrt{3}ln(l^2 + m^2)(dd\delta)$
$d_{x^2-y^2}$	$d_{x^2-y^2}$	$\frac{3}{4}(l^2 - m^2)^2(dd\sigma) + [l^2 + m^2 - (l^2 - m^2)^2](dd\pi) + [n^2 + \frac{1}{4}(l^2 - m^2)^2](dd\delta)$
$d_{x^2-y^2}$	$d_{3z^2-r^2}$	$\frac{1}{2}\sqrt{3}(l^2 - m^2)[n^2 - \frac{1}{2}(l^2 + m^2)](dd\sigma) + \sqrt{3}n^2(m^2 - l^2)(dd\pi) + \frac{1}{4}\sqrt{3}(1 + n^2)(l^2 - m^2)(dd\delta)$
$d_{3z^2-r^2}$	$d_{3z^2-r^2}$	$[n^2 - \frac{1}{2}(l^2 + m^2)]^2(dd\sigma) + 3n^2(l^2 + m^2)(dd\pi) + \frac{3}{4}(l^2 + m^2)^2(dd\delta)$

Table B.2: Interactions from two-centered integrals for $d - d$ orbitals as discussed by Slater and Koster [41]. This utilizes a normalized position vector $\hat{\mathbf{r}} = (l, m, n)$ between interacting orbitals.

Bibliography

- [1] K. S. Novoselov, A. K. Geim, S. V. Morozov, D. Jiang, Y. Zhang, S. V. Dubonos, I. V. Grigorieva, and A. A. Firsov. Electric field effect in atomically thin carbon films. *Science*, 306(5696):666–669, 2004.
- [2] Han Liu, Adam T. Neal, Zhen Zhu, Zhe Luo, Xianfan Xu, David Tománek, and Peide D. Ye. Phosphorene: An unexplored 2d semiconductor with a high hole mobility. *ACS Nano*, 8(4):4033–4041, 2014.
- [3] J. Ribeiro-Soares, R. M. Almeida, L. G. Cançado, M. S. Dresselhaus, and A. Jorio. Group theory for structural analysis and lattice vibrations in phosphorene systems. *Phys. Rev. B*, 91:205421, May 2015.
- [4] Nathanael J. Roome and J. David Carey. Beyond graphene: Stable elemental monolayers of silicene and germanene. *ACS Applied Materials & Interfaces*, 6(10):7743–7750, 2014. PMID: 24724967.
- [5] Liang-Feng Huang, Peng-Lai Gong, and Zhi Zeng. Phonon properties, thermal expansion, and thermomechanics of silicene and germanene. *Phys. Rev. B*, 91:205433, May 2015.
- [6] Qing Peng, Wei Ji, and Suvarna De. Mechanical properties of the hexagonal boron nitride monolayer: Ab initio study. *Computational Materials Science*, 56:11 – 17, 2012.
- [7] Xuemei Li, Jun Yin, Jianxin Zhou, and Wanlin Guo. Large area hexagonal boron nitride monolayer as efficient atomically thick insulating coating against friction and oxidation. *Nanotechnology*, 25(10):105701, feb 2014.
- [8] Yilei Li, Yi Rao, Kin Fai Mak, Yumeng You, Shuyuan Wang, Cory R. Dean, and Tony F. Heinz. Probing symmetry properties of few-layer mos2 and h-bn by optical second-harmonic generation. *Nano Letters*, 13(7):3329–3333, 2013.
- [9] Feng Li, Yuanyuan Qu, and Mingwen Zhao. Germanium sulfide nanosheet: a universal anode material for alkali metal ion batteries. *J. Mater. Chem. C*, 4:8905–8912, 2016.
- [10] Kai Chang, Felix Küster, Brandon J. Miller, Jing-Rong Ji, Jia-Lu Zhang, Paolo Sessi, Salvador Barraza-Lopez, and Stuart S. P. Parkin. Microscopic manipulation of ferroelectric domains in snse monolayers at room temperature. *Nano Letters*, 20(9):6590–6597, 2020. PMID: 32809837.

- [11] Naoki Higashitarumizu, Hayami Kawamoto, Chien-Ju Lee, Bo-Han Lin, Fu-Hsien Chu, Itsuki Yonemori, Tomonori Nishimura, Katsunori Wakabayashi, Wen-Hao Chang, and Kosuke Nagashio. Purely in-plane ferroelectricity in monolayer sns at room temperature. *Nature Communications*, 11:2428, 2020.
- [12] Salvador Barraza-Lopez, Benjamin M. Fregoso, John W. Villanova, Stuart S. P. Parkin, and Kai Chang. Colloquium: Physical properties of group-iv monochalcogenide monolayers. *Rev. Mod. Phys.*, 93:011001, Mar 2021.
- [13] Suman Raj Panday and Benjamin M Fregoso. Corrigendum: Strong second harmonic generation in two-dimensional ferroelectric iv-monochalcogenides (2017 j. phys.: Condens. matter 29 43lt01). *Journal of Physics: Condensed Matter*, 30(17):179501, apr 2018.
- [14] Hua Wang and Xiaofeng Qian. Giant optical second harmonic generation in two-dimensional multiferroics. *Nano Letters*, 17(8):5027–5034, 2017. PMID: 28671472.
- [15] Vicky Jenson and Andrew Adamson (Director). Shrek. DreamWorks Animation, 2001.
- [16] Joseph E. Roll, John M. Davis, John W. Villanova, and Salvador Barraza-Lopez. Elasticity of two-dimensional ferroelectrics across their paraelectric phase transformation. *Phys. Rev. B*, 105:214105, Jun 2022.
- [17] Richard Martin. *Electronic Structure: Basic Theory and Practical Methods*. Cambridge University Press, 2004.
- [18] Martijn Marsmin. Basics: DFT, plane waves, PAW method, electronic minimization: Part 1. In *VASP Workshop at NERSC*, 2016.
- [19] W. Kohn and L. J. Sham. Self-consistent equations including exchange and correlation effects. *Phys. Rev.*, 140:A1133–A1138, Nov 1965.
- [20] Encut - vaspwiki, <https://www.vasp.at/wiki/index.php/encut>.
- [21] Javier Junquera, Óscar Paz, Daniel Sánchez-Portal, and Emilio Artacho. Numerical atomic orbitals for linear-scaling calculations. *Phys. Rev. B*, 64:235111, Nov 2001.
- [22] T. Ozaki. Variationally optimized atomic orbitals for large-scale electronic structures. *Phys. Rev. B*, 67:155108, Apr 2003.
- [23] Martijn Marsmin. VASP: Beyond DFT, The Random Phase Approximation. In *VASP Workshop at NERSC*, 2016.
- [24] M. Shishkin and G. Kresse. Implementation and performance of the frequency-dependent gw method within the paw framework. *Phys. Rev. B*, 74:035101, Jul 2006.
- [25] M. Shishkin and G. Kresse. Self-consistent gw calculations for semiconductors and insulators. *Phys. Rev. B*, 75:235102, Jun 2007.

- [26] M. Shishkin, M. Marsman, and G. Kresse. Accurate quasiparticle spectra from self-consistent gw calculations with vertex corrections. *Phys. Rev. Lett.*, 99:246403, Dec 2007.
- [27] F. Fuchs, J. Furthmüller, F. Bechstedt, M. Shishkin, and G. Kresse. Quasiparticle band structure based on a generalized kohn-sham scheme. *Phys. Rev. B*, 76:115109, Sep 2007.
- [28] Lars Hedin. New method for calculating the one-particle green's function with application to the electron-gas problem. *Phys. Rev.*, 139:A796–A823, Aug 1965.
- [29] G. Kresse and J. Hafner. Ab initio molecular dynamics for liquid metals. *Phys. Rev. B*, 47:558–561, Jan 1993.
- [30] G. Kresse and J. Hafner. Ab initio molecular-dynamics simulation of the liquid-metal–amorphous-semiconductor transition in germanium. *Phys. Rev. B*, 49:14251–14269, May 1994.
- [31] G. Kresse and J. Furthmüller. Efficiency of ab-initio total energy calculations for metals and semiconductors using a plane-wave basis set. *Computational Materials Science*, 6(1):15–50, 1996.
- [32] G. Kresse and J. Furthmüller. Efficient iterative schemes for ab initio total-energy calculations using a plane-wave basis set. *Phys. Rev. B*, 54:11169–11186, Oct 1996.
- [33] G. Kresse and D. Joubert. From ultrasoft pseudopotentials to the projector augmented-wave method. *Phys. Rev. B*, 59:1758–1775, Jan 1999.
- [34] Jiří Klimeš, David R Bowler, and Angelos Michaelides. Chemical accuracy for the van der waals density functional. *Journal of Physics: Condensed Matter*, 22(2):022201, dec 2009.
- [35] Jiří Klimeš, David R Bowler, and Angelos Michaelides. Van der waals density functionals applied to solids. *Phys. Rev. B*, 83:195131, May 2011.
- [36] Hendrik J. Monkhorst and James D. Pack. Special points for brillouin-zone integrations. *Phys. Rev. B*, 13:5188–5192, Jun 1976.
- [37] Arash A. Mostofi, Jonathan R. Yates, Giovanni Pizzi, Young-Su Lee, Ivo Souza, David Vanderbilt, and Nicola Marzari. An updated version of wannier90: A tool for obtaining maximally-localised wannier functions. *Computer Physics Communications*, 185(8):2309–2310, 2014.
- [38] Lidia C. Gomes, P. E. Trevisanutto, A. Carvalho, A. S. Rodin, and A. H. Castro Neto. Strongly bound mott-wannier excitons in ges and gese monolayers. *Phys. Rev. B*, 94:155428, Oct 2016.
- [39] Guangsha Shi and Emmanouil Kioupakis. Anisotropic spin transport and strong visible-light absorbance in few-layer snse and gese. *Nano Letters*, 15(10):6926–6931, 2015. PMID: 26393677.

- [40] José M Soler, Emilio Artacho, Julian D Gale, Alberto García, Javier Junquera, Pablo Ordejón, and Daniel Sánchez-Portal. The siesta method for ab initio order-n materials simulation. *IOP Science*, 14:2745–2779, 2002.
- [41] J. C. Slater and G. F. Koster. Simplified lcao method for the periodic potential problem. *Phys. Rev.*, 94:1498–1524, Jun 1954.
- [42] J. A. Nelder and R. Mead. A Simplex Method for Function Minimization. *The Computer Journal*, 7(4):308–313, 01 1965.